

**Interactive comment on “The El Niño event of 2015–16: Climate anomalies and their impact on groundwater resources in East and Southern Africa” by Seshagiri Rao Kolusu et al. <https://www.hydrol-earth-syst-sci-discuss.net/hess-2018-516/>**

Reviewers' comments in BLACK

Our responses to comments in BLUE (italics are quotes from the paper)

### **Reply to Anonymous Referee 1:**

We would like to thank the reviewer for taking time to review this manuscript thoroughly and for their comprehensive comments received. We have addressed all comments in turn below: We have made all suggested changes in the revised MS.  
(Please see them in blue color text)

This paper compares a leading agro climatic indicator (the SPEI) with other estimates of water availability, over two regions of Africa and specifically focusing on the 2015-16 Southern Africa drought. Overall I found this paper to be very well-written and focused, and using some interesting analysis and data products to characterize the 2015-16 season. I especially liked the use of the IAF curves. I recommend this article for publication.

We thank the reviewer for his/her positive comment and finding our study very interesting.

I have two minor points that I think would help the paper, but I will leave it to the discretion of the authors how to respond to these issues.

First, there are many potential data inputs which could be used for the calculation of SPEI. While these are mentioned in the S2 supplemental material, I think that the manuscript would benefit from moving the first paragraph of the S2 section to the manuscript proper. Stating upfront which precipitation and PET estimates are used will help the manuscript by letting people better understand the historical record being used and the flavor(s) of PET calculation.

We understand the reviewer's comment here. The main paper was deliberately written to be as short as possible, with much of the detail in the supplementary material (SM), increasingly popular in many journals. Of course there is a trade-off between brevity and detail in the main paper. Given this comment and comment 1 of reviewer 2 and comment 2 of reviewer 3 we agree that the methods section should include more detail, and have accordingly moved important components from the SM to the main methods section, as advised.

Secondly, I think the identification of the discrepancies between the GRACE data and the SPEI and GLDAS is quite interesting. While this paper is not meant to be a criticism of those other products, I think it should be noted that they are dramatically different in some locations, and that (typically) the GRACE does not match up with the SPEI. I think if this paper is proposing to use the SPEI to characterize drought events that this might be a useful

opportunity to clarify these discrepancies, and where to put the confidence. This is touched on in the closing of section 3.2.2, by comparing to the piezometry, but I think that this is an important and relevant finding of this paper, and definitely calls into question the use of GRACE for monitoring groundwater.

We agree that the comparison of the SPEI values with GRACE water storage components (and the contributing GLDAS water budget components) is interesting. Indeed our analysis of the structure of apparent qualitative agreement and discrepancy forms Section 3.2.1 in its entirety. We made informed speculation about the potential sources of the discrepancies, supported by our comprehensive analysis of the uncertainties in the estimation of all the quantities considered. To this we have now added additional clarify on the nature of potential errors in GRACE retrievals of dTWS and cite the most recent approaches to address this. Further, as the reviewer notes our comparison of GRACE dGWS with piezometric observations in Section 3.2.2 provides further insight into GRACE TWS errors (see a new plot, Figure S3, in the supplementary material showing individual TWS time-series data from 3 GRACE solutions). We return to the issue in the Conclusion (lines 526-542) and have now strengthened our cautionary inference as suggested by the reviews (line 540-42).

**Interactive comment on “The El Niño event of 2015–16: Climate anomalies and their impact on groundwater resources in East and Southern Africa” by Seshagiri Rao Kolusu et al.**

**Anonymous Referee #2**

**Reply to Anonymous Referee 2:**

**Overall review**

This paper by Kolusu et al. examines different climate and groundwater anomalies in East and Southern Africa related to the period of 2015-2016, which corresponded with one of the worst droughts that occurred in Southern Africa. This study puts in context what were some of the major factors leading up to and affecting the severe drought in Southern Africa and the rainy conditions in East Africa, during this period. The paper overall contributes relevant science questions and results, within the scope of HESS, and presents relevant results that address a key water resource issue (i.e., groundwater depletion and recharge) in a vulnerable climate changing region. Major conclusions are reached in this work, but there are some points that the authors may want to consider addressing in their results and discussion. Some examples are provided below in the “Specific comments” section. The abstract and overall presentation of the paper is clear, however, having so much of the background material in the Supplementary Information document requires the readers to continuously refer to the separate document, interrupting the flow of reading the main manuscript at times. Scientific methods and assumptions are outlined and described well, in both the manuscript and Supplementary Information. The results are overall sufficient to support the authors’ conclusions, and most of the dataset and method descriptions are well explained. Also, proper credit is given to previous studies and data providers.

**Specific comments 1.** The authors place much of the paper’s background and details in the Supplementary Information section. At times, placing some of the information in the main manuscript would actually help the flow of the paper more, instead of the reader having to constantly refer to the supplementary material. Some examples include the background discussion of the SPEI, which almost all is placed in the Supplementary Information section. However, the SPEI is one of the more crucial metrics used to address their science question on the relationship to the groundwater datasets and anomalies.

We agree (as does reviewer #1) and have now moved much of the important detail from the Supplementary Information to the Methods section [see lines - 116-168 and 172-241 in the revised manuscript].

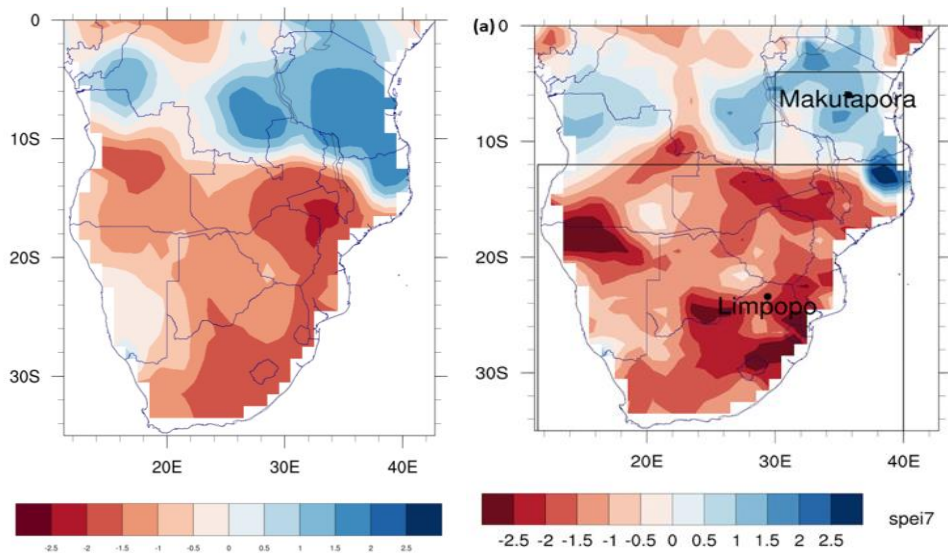
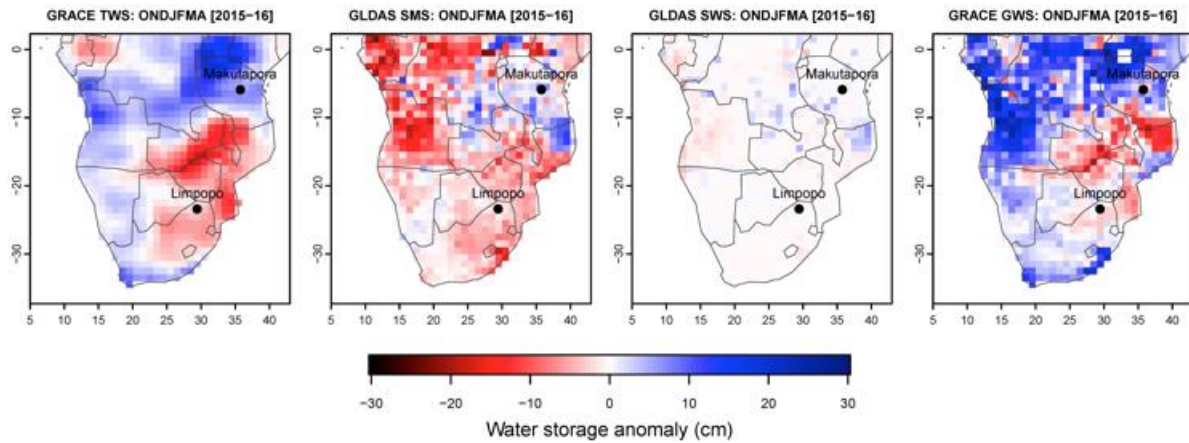
**2.** Lines 230-233: Authors may want to be careful in stating with such certainty that the “2015-2016 magnitude of the SPEI-7 drought over SA . . . increased two times due to the effects purely of anthropogenic warming. . .”. Though anthropogenic warming may be

contributing to greater magnitudes, expressed with such drought metrics, other effects such as persistent drought or dry-land-atmospheric feedbacks could have greatly contributed as well.

We agree that attribution of changing climate risks is challenging. For that reason we consider only the contribution of anthropogenic changes in regional temperature to drought risk, for which we have much greater confidence in attribution than we do for anthropogenic influence on regional rainfall (Bindoff et al. 2013). We hope this is clearly explained in both the description of the attribution method (SM Section S2) and in the results section i.e. ‘*We estimate that the risk of a 2015-16 magnitude SPEI-7 drought over SA to have increased by approximately two times due to the effects purely of anthropogenic warming, ignoring changes to other climate variables and variability*’ (lines 324-6). The role of dryland-atmosphere interaction is to some extent accounted for in our method, since the magnitude of the estimated anthropogenic effect on temperature trends (which drives the SPEI) includes those effects at least as simulated in the climate models. We feel that the greatest uncertainties are likely to be associated with the estimation of the return period values for extreme events and we have now strengthened the caveats around our estimate in Section S2.

**3.** Lines 259-291: The authors report that there are discrepancies between the groundwater water storage (GWS) estimates, involving their three-member GRACE dataset ensemble mean and with the ensemble of SPEI-7 datasets, in both meteorological fields and PET methodologies (e.g., Penman-Monteith vs. Thornthwaite). The question comes up about the different datasets that are used in the SPEI metric methods, i.e., GPCP and CRUTS3.24.01, and different water storage term ensembles, using GLDAS inputs, which use different meteorological datasets, e.g., the GDAS and CMAP-based forcings. Could these factor into the differences seen between the SPEI anomalies and deltaSMS and deltaGWS anomalies? Also, the SPEI is derived based on the data record from 1901 to present, which would be a different period from the GRACE measurements (2002-2016) and then again for the GLDAS datasets (2000-present, if using GDAS). Authors may want to address these possible discrepancies as well.

The reviewer raises a similar point to the first comment of reviewer 1 and we refer to our response to that. In specific response to the query about the potential difference between SPEI-7 derived from GPCC vs CMAP data we have now done that comparison (see below) and note that our the pattern of inconsistency between SPEI-7 and GRACE remains, which we consider in Section 3.2.1. The issue of the differing relative magnitudes of SPEI-7 and TWS anomalies over South Africa is less apparent with SPEI-7(CMAP) and we note that in point (i) in para 2 of Section 3.2.1 (lines 389-391)



Finally, in relation to their results and discussion on this topic, the authors may want to consider that the time windows relevant to the SPEI fields and those of GRACE, and other LSM-based fields, can be different and that the recharge or other drawdowns of groundwater can vary and take time in response to the rainy season. The authors point out this lag in lines 304-306 in relation to figure 5. The October-April SPEI timeframe may not have exactly aligned with the GRACE-ensemble (e.g., deltaTWS) and LSM ensemble (e.g., deltaSMS), as the response to the lower layers may be better reflected in a lagged timeframe (e.g., December-June). Also, trends in the TWS may already have been present that the SPEI-7 may not have captured, given the differences in datasets. Authors may want to look at other studies that have addressed such issues, such as Hassan and Jin (2016), Rodell et al. (2018), and Zhao et al., 2017:

[We note this point now in Section 3.1.2 \(lines 385-390\) and cite the suggested references.](#)

**4.** Lines 323-325: The authors mention here that the GRACE ensemble-based deltaGWS in the early part of the 2015-2016 drought had a high amount of uncertainty and did not correspond well with the piezometry data for the Limpopo site region. It would be of interest

here if they could identify which of the three GRACE TWS anomaly products contributed to the higher blue shaded region in the last half of 2015. Note the lower minimum values of the ensemble spread show some steep decline from late 2015 into 2016. Though the authors do point to the Scanlon et al. (2018) study in lines 302-303 of the Supplementary Information document, it would be of interest to the community to know which product contributed to this GWS reduction.

We thank the reviewer for highlighting the uncertainty in GRACE TWS signals for the Limpopo Basin particularly for the period of 2015-16. We did note in the SM that there is some indication from Fig. S2, that during such periods of greatest  $\Delta GWS$  uncertainty, it is the uncertainty in GRACE  $\Delta TWS$  that makes most important contribution, rather than uncertainty in the GLDAS components. We have now looked at the individual TWS time-series data for 3 GRACE products of CSR, JPL-Mascon and GRGS (Fig. S3 reproduced below). We confirm that differences among the three GRACE products for the 2015-16 period are substantial. We note that (i) for late 2015 it is the GRGS product which is largely responsible for the poor correspondence between piezometry and the GRACE mean  $\Delta GWS$  retrieval, as GRGS, unlike the other two products shows a substantial increase in  $\Delta GWS$ . (ii) During early 2016 it is the JPL-Mascon (MSCN) product that deviates from the other two showing continued negative anomalies whereas both CSR and GRGS feature slightly positive anomalies. We provide this new plot of GRACE TWS time-series data for both Limpopo and Makutapora basins in the revised supplementary material (Fig. S3) and make appropriate reference in the main text of Section 3.2.2 para 3.

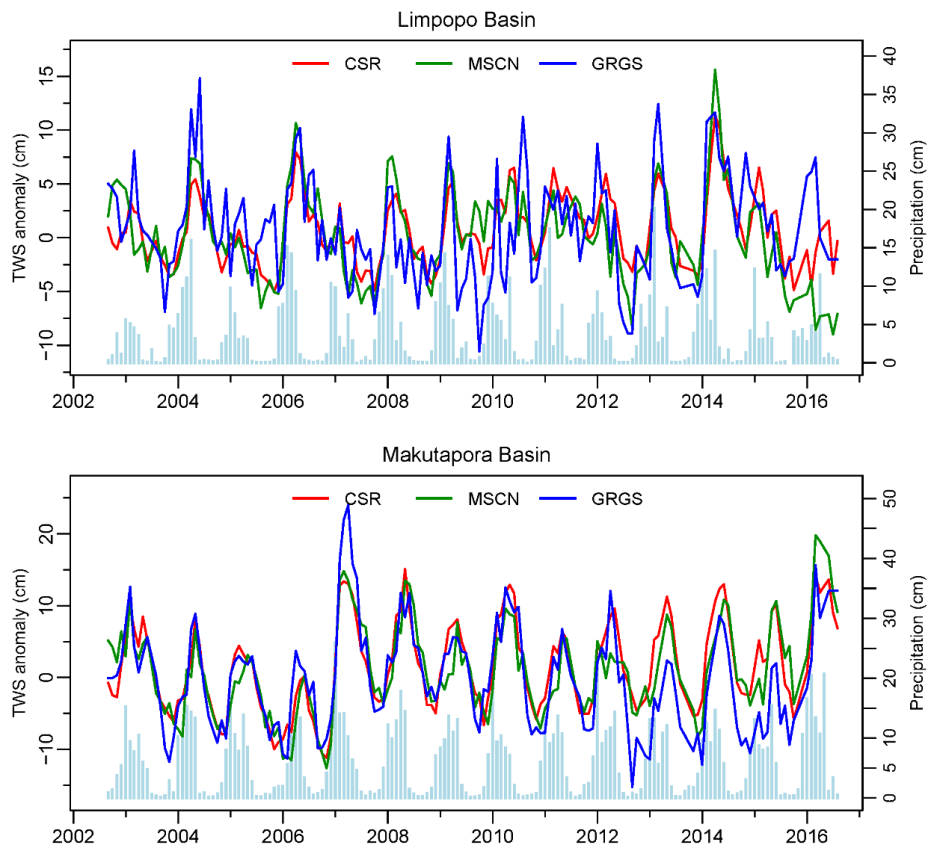




**Figure S3:** (a) Time series of estimates of monthly  $\Delta$ TWS anomaly (cm) at Limpopo from August 2002 to July 2016 (averaged over an area approximately  $\sim 120\,000\text{ km}^2$ ) derived from the three individual GRACE retrievals of CSR (red), JPL-Mascons (green) and GRGS (blue). Monthly rainfall (from GPCP product, cm) shown as bars. (b) As (a) but for Makutapora.

**Technical corrections Main manuscript: 1.** Lines 96 and 111: Noticed that authors use “EASA” instead of “EASE” for the northern of the two domains in these two lines. They should be replaced with “EASE”?

Corrected

2. Line 161: Should the reference to “figure S1(b)” actually be to “figure S1(d)”, if highlighting the SST anomalies associated with this 7-month period?

Corrected

3. Line 217: Authors may want to replace the article “an” in front of “East Pacific” with either “than” or “in” here.

Corrected

4. Lines 221-222: The last phrase of this sentence is not fully clear: “and statistically this 2-year drought event remarkably unlikely”. Please clarify what is meant here.

The return period estimates for a consecutive 2-year SPEI-7 IAF curves for 2014-16 are extremely high such the uncertainty is too poorly constrained to have confidence. So we prefer not to provide the absolute values

5. Line 315: Remove the comma after “GWS” and before “suggests”.

Corrected

6. Lines 341-344: This sentence is a bit awkward in places, e.g., “The magnitude of major GRACE increases in deltaGWS”, or “with no response apparent in piezometry.” It is recommended to improve these phrases and overall clarity of the sentence.

Corrected

7. Lines 358-362: This is a long run-on sentence, and it is recommended to break this sentence in to two separate ones to improve its readability.

Corrected

8. Line 404: Place the period after the “l” in “et al., 2018).

Corrected

9. Figure 1b: It is unclear about how the 80th percentile of the rainfall anomalies is established. Is this constructed relative to the EASE box? Please clarify further how the positive and negative anomalies are established in Figure 1b (in the main text) relative to the 80th percentile.

This is now explained in the methods section

10. Figure 3 caption, line 619: “men” should be changed to “mean”.

Corrected

**Supplementary manuscript:**

1. Line 107: “EASA” occurs here as well.

Corrected

2. Line 116: “Penman-Montieth” should be spelled: “Penman-Monteith”.

Corrected

3. Line 124: Can remove either “use” or “derive” in front of “percentiles”.

Corrected

4. Line 125: The authors may want to provide the full name for TRMM 3B42 product, not just the acronym for the satellite and precipitation product. Also, it may be helpful to specify here which years of the TRMM product were used.

Corrected

5. Caption for Figure S1: The final sentence description for S1-d seems incomplete. What period was the anomalies derived from?

Information provided

6. Figure S2a, for Limpopo location, the shading in the top four panels is missing, unlike that for S2b, which shows the shading in those panels for Makutapora. Also, recommend placing the word “and” between “(a) Limpopo” and “(b) Makutapora”.

Shading is included in both (a) and (b).



### Anonymous Referee #3

Overall its a good paper. I am happy that they treated the 2015-16 drought in context of the dryness of the previous year, this was one of the points I was looking for.

We thank the reviewer for his/her positive assessment.

1. However, given one of their introductory lines: "Few studies have investigated the hydrological impacts of ENSO events on groundwater despite its vital role in sustaining ecosystem function as well as agricultural and domestic water supplies" (line 60-62), I thought they would proceed to do that very investigation which as they mentioned is lacking. I think this statement (line 60-62) should either be removed, or they should explicitly mention that they also do not do this investigation.

Statement now removed as advised

2. Also, a brief background on how the GRACE estimates are derived would be helpful for C1 the readers who are less knowledgeable on climate issues, as this paper could have considerable interest from hydrologists

We agree and not similar comments from reviewers 1 and 2. Accordingly We have now moved the description of the methodology to retrieve GWS from GRACE data from the supplementary material to the methods section of the manuscript (Section 2.2)

3. Line 59: Are not other phenomenon like QBO, MJO etc also major drivers. The way it is written suggest ENSO is the only major driver. Line 65: "strongest" rather than "biggest", perhaps?

We have now clarified this statement and referred directly to section S1 of the supplementary material in which we discuss the various major modes of variability across our study domain (see lines 60-61 and 68)

4. Line 91: "temporally", rather than "temporarily"?

Corrected as suggested

5. Line 221-222: the grammar needs to be corrected, perhaps: "this 2 year drought event [is] remarkably unlikely" (ie, add the word: "is")

Corrected as suggested

6. Line 315-316: It is not clear whether the  $r$  of 0.62 is for annual or seasonal? It may be instructive to calculate separate  $r$  values for Makutapora and Limpopo, since they are dealing with only 2 sites. Scatter plots would also be a helpful addition.

Clarified as suggested in lines 429-430 and 464. In order to limit the number of Figures we prefer not to show the scatterplots

7. Line 319: remove the word "least"?

Corrected as suggested

8. Line 328-329: the phrase "shows little interannual variability" should perhaps be replaced by "shows a limited interannual cyclicality"

Revised

9. Line 339: The colour scheme on Figure S1 d is a little unusual, in most color schemes red is warmer and blue is colder, this can confuse readers.

Corrected as suggested

10. Line 387-388 need to be revised gramatically.

Corrected as suggested

11. Line 402-403: further analysis is required to support this sentence: "although as our results at Limpopo show, consecutive dry years lead to marked storage reduction"; this can be achieved by for example, by comparing with the storage after another dry year that was in contrast preceded by wet conditions.

We believe that it is clear from Figure 5 that the very weak recharge during 2014-15 and 2015-16 leads to the lowest GWS values on record.

12. Line 420-432: A mention of the use of seasonal climate forecasts along with climate drivers would be helpful, as these seasonal forecast tend to try to bring together the effects of various parameters including climate modes like ENSO, IOD etc.(such forecasts as the ones here:  
[http://www.cpc.ncep.noaa.gov/products/international/nmme/nmme\\_seasonal\\_body.html](http://www.cpc.ncep.noaa.gov/products/international/nmme/nmme_seasonal_body.html))

This is a good point and we have now included this suggestion. (lines 535-536)

13. Line 639; Fig 5b and 5c. The authors can potentially answer the question of whether GRACE GWS better estimates abstraction rates + borehole GWS by adding the two

We welcome this constructive suggestion to better compare borehole GWS to GRACE GWS. There is one important confounding factor that inhibits the success of implementing this straight-forward suggestion: transience in the response of groundwater levels (i.e. groundwater storage) to changes in pumping from the Makutapora Wellfield. Co-authors Seddon, Taylor and Cuthbert have been working on the development of a numerical model to better represent transience in groundwater-level responses and thus produce a time series record of groundwater levels for the Makutapora Wellfield in which the impacts of pumping have been removed. This work is on-going and they hope to report soon on their results. We will thus leave the observed, uncorrected groundwater-level time series in Figure 5 as it is with all of the associated commentary on the observed impacts of pumping on this groundwater-level record.

1 **The El Niño event of 2015-16: Climate anomalies and their impact on groundwater**  
2 **resources in East and Southern Africa**

3

4 Seshagiri Rao Kolusu<sup>1</sup>, Mohammad Shamsudduha<sup>2,3</sup>, Martin C Todd<sup>1</sup>, Richard G Taylor<sup>2</sup>,  
5 David Seddon<sup>2</sup>, Japhet J Kashaigili<sup>4</sup>, Girma Y Ebrahim<sup>5</sup>, Mark O Cuthbert<sup>2,6</sup>, James P R  
6 Sorensen<sup>7</sup>, Karen G Villholth<sup>5</sup>, Alan M MacDonald<sup>8</sup>, and Dave A MacLeod<sup>9</sup>

7

8 1. Department of Geography, University of Sussex, Brighton, BN1 9QS, UK

9 **Correspondence:**[s.kolusu@sussex.ac.uk](mailto:s.kolusu@sussex.ac.uk) and [sesukulusu@gmail.com](mailto:sesukulusu@gmail.com)

10 2. Department of Geography, University College London, Gower Street, London WC1E  
11 6BT UK

12 3. Institute for Risk and Disaster Reduction, University College London, Gower Street,  
13 London WC1E 6BT, UK

14 4. Sokoine University of Agriculture, Morogoro, Tanzania

15 5. International Water Management Institute, Pretoria, South Africa

16 6. School of Earth and Ocean Sciences, Cardiff University, Main Building, Park Place,  
17 Cardiff, CF10 3AT, UK

18 7. British Geological Survey, Maclean Building, Crowmarsh Gifford, Wallingford,  
19 Oxfordshire OX10 8BB UK

20 8. British Geological Survey, The Lyell Centre, Research Avenue South, Edinburgh  
21 EH14 4AP UK

22 9. Atmospheric Oceanic and Planetary Physics, University of Oxford, OX1 3PU,UK

23

24 **Keywords**

25

26 El Nino; ENSO; Climate; groundwater; Africa; sustainability; recharge; climate impacts; water  
27 management; GRACE

28

29 **Abstract**

30

31 The impact of climate variability on groundwater storage has received limited attention despite  
32 widespread dependence on groundwater as a resource for drinking water, agriculture and  
33 industry. Here, we assess the climate anomalies that occurred over Southern Africa (SA) and  
34 East Africa, south of the equator (EASE), during the major El Niño event of 2015-16, and their  
35 associated impacts on groundwater storage, across scales, through analysis of in situ  
36 groundwater piezometry and GRACE satellite data. At the continental scale, the El Niño of  
37 2015-16 was associated with a pronounced dipole of opposing rainfall anomalies over EASE  
38 and Southern Africa, north/south of  $\sim 12^{\circ}\text{S}$ , a characteristic pattern of ENSO. Over Southern  
39 Africa the most intense drought event in the historical record occurred, based on an analysis of  
40 the cross-scale areal intensity of surface water balance anomalies (as represented by the  
41 Standardised Precipitation-Evapotranspiration Index, SPEI), with an estimated return period of  
42 at least 200 years and a best estimate of 260 years. Climate risks are changing and we estimate  
43 that anthropogenic warming only (ignoring changes to other climate variables e.g.  
44 precipitation) has approximately doubled the risk of such an extreme SPEI drought event.  
45 These surface water balance deficits suppressed groundwater recharge, leading to a substantial  
46 groundwater storage decline indicated by both GRACE satellite and piezometric data in the  
47 Limpopo basin. Conversely, over EASE during the 2015-16 El Niño event, anomalously wet  
48 conditions were observed with an estimated return period of  $\sim 10$  years, likely moderated by  
49 the absence of a strongly positive Indian Ocean Zonal Mode phase. The strong but not extreme  
50 rainy season increased groundwater storage as shown by satellite GRACE data and rising  
51 groundwater levels observed at a site in central Tanzania. We note substantial uncertainties in  
52 separating groundwater from total water storage in GRACE data and show that consistency  
53 between GRACE and piezometric estimates of groundwater storage is apparent when spatial  
54 averaging scales are comparable. These results have implications for sustainable and climate-  
55 resilient groundwater resource management, including the potential for adaptive strategies,  
56 such as managed aquifer recharge during episodic recharge events.

## 57 **1. Introduction**

58

59 The El Niño-Southern Oscillation (ENSO) phenomenon is the dominant single driver of  
60 interannual climate variability and large-scale extremes across the tropics including much of  
61 Africa. Few studies have investigated the hydrological impacts of ENSO events on  
62 groundwater. Here, we quantify climate anomalies and groundwater resources over Eastern  
63 Africa, South of the Equator (EASE) and Southern Africa (SA), during the recent major El  
64 Niño event of 2015-16, which in the Pacific sector was one of the strongest on record. El Niño  
65 is typically associated with wet and dry anomalies over EASE and SA, respectively  
66 (Ropelowski and Halpert, 1987), but with considerable diversity in this response among El  
67 Niño events, in part related to the many other drivers of variability active over EASE and SA  
68 (Supplementary Information S1). Much of SA experienced extreme drought in 2015-16 with  
69 severe impacts on local food security, livelihoods and key sectors of the economy (SADC  
70 2016a; 2016b; Archer *et al.*, 2017; Siderius *et al.*, 2018; Supplementary Information S1).

71

72 Groundwater is the dominant source of safe water for rural populations and many expanding  
73 cities in EASE and SA (MacDonald *et al.*, 2012); in drylands, groundwater is often the only  
74 perennial source of water. Although relatively under-developed to date, groundwater resources  
75 are being developed rapidly in Africa (Taylor *et al.*, 2009; Calow *et al.*, 2010; Villholth *et al.*,  
76 2013) and feature prominently in national development plans, especially to satisfy the need for  
77 increased access to safe water and agricultural intensification under rapidly growing  
78 populations and economic development. Groundwater is especially important in Africa where  
79 surface runoff efficiency is lower than elsewhere (McMahon *et al.*, 1987) and drinking of  
80 untreated surface water is associated with poor health (Hunter *et al.*, 2010). The long-term  
81 viability of groundwater withdrawals and the livelihoods and ecosystems that groundwater  
82 sustains depend on recharge.

83

84 Unlike surface water, research evaluating associations between groundwater storage and  
85 ENSO, or indeed other modes of climate variability is rather limited (e.g. Holman *et al.*, 2011,  
86 Kuss and Gurdak, 2014), despite evidence that climate variability and extreme rainfall  
87 preferentially drive or restrict groundwater recharge. Several studies have shown recharge to  
88 be episodic in semi-arid regions of Africa (Meyer *et al.*, 2005, van Wyk *et al.*, 2011, Taylor *et*

89 *al.*, 2013, Cuthbert *et al.*, 2017) and elsewhere (Jasechko and Taylor, 2015, Cuthbert *et al.*,  
90 2016), highlighting the need to understand patterns and drivers of climate variability both  
91 temporally and spatially, that influence recharge. Bonsor *et al.* (2018) analysed recent (2002-  
92 2016) trends in, and seasonality of groundwater storage within 12 African sedimentary basins  
93 implied from GRACE satellite data. Here, we employ evidence from both in situ observations  
94 (piezometry) and GRACE satellite data to examine the effect of large-scale interannual climate  
95 anomalies on groundwater across spatial scales for locations and domains that represent the  
96 rainfall anomaly gradient over EASE and SA associated with characteristic El Niño response,  
97 exemplified by the event of 2015-16. Beyond a few site-specific studies, the impacts of larger-  
98 scale climate extremes on groundwater remain substantially unresolved. This hinders our  
99 ability to determine acceptable levels of groundwater abstraction and depletion. This study  
100 aims to quantify and understand the responses, during the 2015-16 El Niño of (i) the  
101 surface/terrestrial water balance and (ii) groundwater storage over EASE and SA from regional  
102 to local scales. Further, it seeks to place the 2015-16 El Niño event statistically in the historical  
103 context.

104

## 105 **2. Data and methods**

106

### 107 2.1. Climate data and analysis

108

109 We analyse data over the broad region of Africa South of the Equator and over an extended  
110 austral summer wet season of October-April, which encompasses the full wet season over SA  
111 (excluding the Cape region) and those parts of EASE (south of  $\sim 5^{\circ}\text{S}$ ), which experience a  
112 similarly annual unimodal rainfall regime (Dunning *et al.*, 2016), and will accommodate the  
113 response time of groundwater systems to climate. This region also experiences a coherent  
114 ENSO signal (Section 3.1).

115

116 We use the Standardized Precipitation Evapotranspiration Index (SPEI) (Vicente-Serrano *et al.*  
117 *al.*, 2010), which is a simple representation of surface water balance anomalies, derived over  
118 this 7-month season (SPEI-7), over the period 1901 to present using precipitation data from the  
119 Global Precipitation Climatology Centre (GPCC) monthly product v7 (Schneider *et al.*, 2011;  
120 2014) at  $1.0^{\circ}$  resolution. To account for uncertainty in estimation of PET we use three

121 parameterisations of varying complexity: The Penman-Monteith equation, based on net  
122 radiation, temperature, wind-speed and vapour pressure); The Hargreaves equation, based on  
123 mean, minimum and maximum temperature and extra-terrestrial solar radiation; The  
124 Thornthwaite equation, which is based solely on surface air temperature. The variables required  
125 for the various PET estimates are obtained from the CRUTS3.24.01 dataset (Harris *et al.*,  
126 2014). Note that some findings will be sensitive to this choice of drought index.

127

128 SPEI-7 anomalies are analysed for two large sub-domains, specifically EASE (4-12°S, 30-  
129 40°E) and SA (10-35°S, 10-40°E) which encompass the anomalous wet and dry dipole  
130 conditions, respectively, typically experienced during El Niño events (Fig. S1(b)) and  
131 specifically in 2015-16 (Fig. 1(a)). For each domain, the areal extent and intensity of SPEI-7  
132 in each year of the record was characterised using Intensity-Areal-extent Frequency (IAF)  
133 curves of Mishra and Cherkauer (2010). IAF curves show the mean SPEI-7 value of grid cells  
134 lying within various areal extent intervals: The areas covered by the lowest (for SA) or highest  
135 (for EASE) 5th, 10th, 20th...100th areal percentiles of SPEI-7 grid cell values within the  
136 domain area i.e. when all grid cells are ranked. The SPEI-7 IAF curves allow comparison  
137 between years, irrespective of the precise spatial location of dry/wet anomalies within the  
138 domain. This comparison includes estimating the return period of the SPEI-7 IAF curve  
139 observed during the 2015-16 El Niño and other El Niño events. This is achieved by comparing  
140 these observed SPEI-7 IAF curves to curves representing various benchmark return periods,  
141 derived using a block maximum method applied to SPEI-7 data from a large ensemble of  
142 climate model runs (see Supplementary Information S2).

143

144 It is likely that anthropogenic climate change is, and will continue to, affect large-scale  
145 hydrology (Bindoff *et al.*, 2013). Here we estimate the effects purely of anthropogenic  
146 temperature trends on drought risk over SA through a simplified attribution experiment. The  
147 SPEI-7 IAF return period analysis above is repeated, but with respect to benchmark return  
148 period IAF curves for which the temperature data, used in calculating PET, has the signal of  
149 anthropogenic climate change removed (see Supplementary Information S2). As such, the  
150 return period of the SPEI-7 IAF curve for 2015-16 is estimated in the context of the ‘real  
151 historical’ world and for comparison in the context of a counterfactual climate with only natural  
152 variability in temperature.



153

154 There is evidence to indicate recharge is preferentially driven by intense rainfall (see references  
155 in Sections 1 and 3.1.1). To examine the nature of rainfall intensities over EASE during the El  
156 Niño 2015-16 event we derive percentiles of the daily rainfall probability distribution from the  
157 Tropical Rainfall Monitoring Mission (TRMM) 3B42 product during the (October-April  
158 season, 1997-2016). In the absence of robust knowledge of actual rainfall thresholds associated  
159 with groundwater recharge, and the likelihood that such thresholds are highly variable in space  
160 and time, we derive the 80<sup>th</sup> percentile of daily rainfall within the season, at each grid cell as a  
161 coarse proxy for rainfall events likely to be associated with recharge. Our results (Section 3.1.1)  
162 are largely insensitive to the choice of percentile value (not shown). We derived the value of  
163 the 80<sup>th</sup> percentile from all the (October-April) data and then just for the 2015-16 season and  
164 show the anomalies. Finally, Information on the large-scale atmospheric circulation is  
165 diagnosed from the horizontal and vertical winds, and specific humidity from ERA-Interim  
166 reanalysis data (Dee *et al.*, 2011). SST data are obtained from the extended reconstructed sea  
167 surface temperature (ERSST) version 4 from the National Oceanographic and Atmospheric  
168 Administration (NOAA) (Smith *et al.*, 2008) on a 2° grid.

169

## 170 2.2 Groundwater storage estimates from GRACE satellite data

171

172 Regional-scale changes in groundwater storage (GWS) (2002-16) are estimated from GRACE  
173 satellite measurements of total terrestrial water storage (TWS) anomalies, by subtracting  
174 changes in the other terrestrial stores, which, in our tropical region, comprise soil moisture  
175 (SMS) and surface water (SWS) stores (eq.1), themselves estimated from Land-Surface Model  
176 (LSM) simulations, in the absence of in situ  $\Delta$ SMS and  $\Delta$ SWS data in the study areas.

177

$$178 \quad \Delta\text{GWS} = \Delta\text{TWS} - (\Delta\text{SMS} + \Delta\text{SWS}) \quad (\text{eq. 1})$$

179 Where  $\Delta$  refers to the anomaly with respect to the long-term data series. To help interpretation  
180 of the mean  $\Delta$ GWS signals we also present the total uncertainty in estimates of  $\Delta$ GWS, which  
181 results from the uncertainty in estimates of  $\Delta$ TWS,  $\Delta$ SMS and  $\Delta$ SWS. Regarding uncertainty  
182 in  $\Delta$ TWS associated with different GRACE processing strategies, we apply an ensemble mean  
183 of three GRACE  $\Delta$ TWS estimates. Namely, the CSR land (version RL05.DSTvSCS1409,  
184 Swenson and Wahr, 2006; Landerer and Swenson, 2012) and JPL Global Mascon (version

185 RL05M\_1.MSCNv01, Watkins *et al.*, 2015; Wiese *et al.*, 2015) solutions, from NASA's  
186 *GRCTellus* data dissemination site (<http://grace.jpl.nasa.gov/data>), and a third GRGS GRACE  
187 solution (CNES/GRGS release RL03-v1) (Biancale *et al.*, 2006) from the French Government  
188 space agency, Centre National D'études Spatiales (CNES). Further information on the  
189 processing involved in each product is provided in Supplementary Information S3. The  
190 monthly GRACE  $\Delta$ TWS are interpolated to a 1-degree grid for analysis in Equation 1. For  
191 analysis of GRACE  $\Delta$ TWS data at the locations of the two groundwater-level monitoring sites  
192 of interest (Makutapora and Limpopo, see below) the monthly  $\Delta$ TWS time-series are generated  
193 by averaging over a 200 km radial buffer (i.e. area equivalent of  $\sim 120\,000\text{ km}^2$ ) around each  
194 location.

195  
196 Further, to account for uncertainty in  $\Delta$ SMS and  $\Delta$ SWS we use data from four LSMs within  
197 NASA's Global Land Data Assimilation System (GLDAS), and provide the associated  
198 uncertainty ranges for each term. GLDAS is an uncoupled land surface modelling system that  
199 includes multiple global LSMs driven by surface meteorology from the NCEP data assimilation  
200 system, CMAP disaggregated precipitation and the Air Force Weather Agency satellite-derived  
201 radiation fields (Rodell *et al.*, 2004). The four GLDAS LSMs are: The Community Land Model  
202 (CLM, version 2) (Dai *et al.*, 2003), NOAH (version 2.7.1) (Ek *et al.*, 2003), the Variable  
203 Infiltration Capacity (VIC) model (version 1.0) (Liang *et al.*, 2003), and MOSAIC Mosaic  
204 (version 1.0) (Koster and Suarez, 1992). Further discussion of the uncertainty in these  
205 individual water balance components (Fig. S2) and further information on the LSMs is  
206 provided in Supplementary Information S3.

207

208

### 209 2.3 Groundwater storage estimates from piezometric observations

210

211 Groundwater-level time series records were compiled in two areas situated at the heart of the  
212 EASE/SA ENSO rainfall dipole centres of action (Fig. 1(a)). (i) The Makutapora wellfield  
213 ( $35.75^\circ\text{E}$ ,  $5.90^\circ\text{S}$ ) site in central Tanzania, East Africa. Groundwater records were collated  
214 from the Ministry of Water and Irrigation and the Dodoma Urban Water Supply, Tanzania.  
215 Here, groundwater is abstracted from an aquifer comprising deeply weathered granite overlain  
216 by alluvium (Taylor *et al.*, 2013). Data from three sites in the wellfield met the data quality

217 criteria and are averaged together; mean groundwater-level time series records were converted  
218 to monthly anomalies in GWS using an in-situ derived specific yield ( $S_y$ ) value of 0.06 (Taylor  
219 *et al.*, 2013). We estimate that these data are representative of groundwater levels across an  
220 area of  $\sim 60 \text{ km}^2$ . (ii) Limpopo Basin in Southern Africa ( $\sim 28$  to  $32^\circ\text{E}$ ,  $22.5$  to  $25^\circ\text{S}$ ).  
221 Groundwater-level records from 40 stations within weathered hard-rock (“basement”) aquifers  
222 in sub-basins A6 (Mogalakwena), A7 (Sand), A8 (Nzhelele) and A9 (Luvuvhu) of the Limpopo  
223 Basin were collated from the Department of Water and Sanitation, Directorate Surface and  
224 Groundwater Information, South Africa. The data were first standardised then averaged  
225 together and represent an area estimated to be  $\sim 47\,000 \text{ km}^2$ . For both sites daily to monthly  
226 groundwater-level records within our common study period of August 2002 to July 2016, were  
227 checked for consistency (missing data less than 10%) and selected for groundwater storage  
228 analysis. Mean groundwater-level time series records were converted to monthly anomalies in  
229 GWS using a  $S_y$  value that produced the lowest root-mean square error between in situ and  
230 GRACE GWS; the applied value (0.025) is consistent with that estimated for basement aquifers  
231 in Africa by MacDonald *et al.* (2012).

232

233 We acknowledge that our estimates of GWS from piezometry may be influenced by  
234 abstractions and we provide data on pumping rates from Makutapora (Fig. 5(c)). A numerical  
235 method to remove the effects of pumping is currently the subject of ongoing research by the  
236 authors, so in this case we infer the effect of pumping on GWS only in only relative qualitative  
237 terms. Equivalent direct data on direct pumping rates is not available at Limpopo. However,  
238 we note that Cai *et al.* (2017) mapped the spatial extent of irrigation across the Limpopo basin  
239 in South African using satellite data and estimated that irrigation from groundwater provides  
240 about 50% of the irrigated areas over 2% of the land area, which likely influences groundwater  
241 storage locally.

242

### 243 **3. Results and discussion**

244

#### 245 3.1 Climate anomalies over EASE and SA during the 2015-16 El Niño event

246

##### 247 *3.1.1 EASE/SA climate anomalies*

248

249 The 2015-16 El Niño was the second strongest event within the available ~165-year Pacific  
250 Ocean Sea Surface Temperature (SST) record, with SST anomalies exceeding 2°C for 6 months  
251 from October 2015 (Fig. S1(d)). By some measures 2015-16 was the strongest El Niño since  
252 1950 (Supplementary Information S1). Many of the observed climate anomalies around the  
253 world were typical of El Niño years (Blunden and Arndt 2016). Over our study region, a  
254 pronounced north-south dipole in SPEI-7 anomalies was observed (Fig. 1(a)), indicating  
255 intense and extensive drought over SA (negative SPEI-7) and the wetter than normal conditions  
256 over EASE (positive SPEI-7). In detail, most of SA south of 10°S experienced a substantial  
257 water balance deficit: exceptional drought (SPEI <-2) conditions were experienced over  
258 extensive parts of northern South Africa and northern Namibia, southern Botswana and  
259 Zambia, as well as most of Zimbabwe and southern Mozambique and Malawi (Fig. 1(a)). Most  
260 of EASE experienced above average rainfall during this period, with SPEI values >1 across  
261 most of Tanzania, and a localised exceptionally wet region over the northernmost part of  
262 Mozambique. The Makutapora and Limpopo sites (Fig. 1(a)) are located in areas representative  
263 of the large-scale north/south rainfall dipole.

264

265 This spatial dipole pattern is very similar to the characteristic pattern of anomalies during El  
266 Niño across the region, as represented by the leading Empirical Orthogonal Function (EOF) of  
267 interannual variability (Fig. S1(b), Section S1) which correlates strongly with ENSO and  
268 Indian Ocean SSTs Fig. S1(c). Indeed, the EOF coefficient value for 2015-16 is the second  
269 highest within the entire 1901-2016 period. As such, across our study region 2015-16  
270 represents an extreme exemplar of the characteristic El Niño climate response. Of course, a  
271 complex set of planetary, regional and local scale processes related to, and independent of, El  
272 Niño are fully responsible for the observed anomalies (e.g. Blamey *et al.*, 2018). The structure  
273 of the atmospheric anomalies, specifically the mean meridional overturning circulation  
274 associated with the large-scale SPEI-7 anomalies (Fig. 2(a)) shows large-scale anomalous  
275 ascent over EASE between ~0° and 10°S indicative of enhanced deep convection, with  
276 compensating descent over SA throughout the depth of the troposphere, which acts to suppress  
277 convection. The low-level horizontal circulation (Fig. 2(b)) indicates key features associated  
278 with the SPEI-7 dipole, notably: (i) An anomalous southerly flow from the southern Indian  
279 Ocean into continental SA (Feature A in Fig. 2(b)), which weakens the transport of water  
280 vapour from the humid tropical Indian Ocean leading to a decrease in moisture flux

281 convergence over SA. This is associated with a weakening of the mean ‘Mascarene’ subtropical  
282 high over the Southern Indian Ocean (Feature B in Fig. 2(b)). (ii) Over EASE there are  
283 anomalous low-level westerlies over Tanzania (Feature C in Fig. 2(b)), which weaken the mean  
284 easterlies and enhance convergence over Tanzania, a structure characteristic of wet spells  
285 (Berhane and Zaitchik, 2014; Nicholson 2017).

286

287 Groundwater recharge in the semi-arid tropics is favoured by high intensity rainfall events  
288 (Owor, 2009; Jasechko and Taylor, 2015) within wet seasons, which may be modulated by  
289 climate anomalies during El Niño conditions. During 2015-16, the intensities of the 80th  
290 percentile of daily rainfall, a simple proxy of potential groundwater recharge-relevant rainfall,  
291 increased by  $\sim 1\text{-}5 \text{ mm day}^{-1}$  across much of EASE (Fig. 1(b)), representing a 100-150%  
292 increase in many places. Whilst the association of rainfall intensity and enhanced recharge  
293 across large and heterogeneous regions remains to be resolved, this intensification of rainfall  
294 is consistent with greater groundwater recharge. Across SA the magnitude of the 80th  
295 percentile reduced by  $\sim 1\text{-}2 \text{ mm day}^{-1}$ , potentially reducing groundwater recharge.

296

### 297 *3.1.2. The 2015-16 event in the historical context*

298

299 SPEI-7 IAF curves represent water balance anomalies across all spatial scales. For the SA  
300 region, 2015/16 experienced the most extreme SPEI-7 drought within the historical period,  
301 with an estimated IAF curve return period of  $\sim 260$  years (range 190-290 years) (Fig. 3(a)). The  
302 2015-16 drought was of greater intensity than those during previous El Niño events of  
303 comparable magnitude, 1997-98 and 1982-83, whose SPEI-7 IAF curve return periods are  
304 estimated to be only  $\sim 6$  years (range 4-9 years) and  $\sim 43$  years (range 35-47 years),  
305 respectively). The contrasting intensity of SA drought between these events highlights the  
306 diversity in responses over EASE/SA to El Niño, related to both the different character of the  
307 events in the Pacific sector (2015-16 was strongest in the central rather than East Pacific as in  
308 1997-98, see Section S1), and the specific regional circulation features during these events  
309 which modulate the diverse ENSO teleconnections to SA (Ratnam *et al.*, 2014; Blamey *et al.*,  
310 2018). Moreover, the 2015-16 drought followed a moderate drought in 2014-15 (Blamey *et al.*,  
311 2018), which had important implications for groundwater levels (Section 3.2.2), and  
312 statistically this 2-year drought event is remarkably unlikely. The extreme SPEI-7 anomalies

313 over SA in 2015-16 result from low rainfall and extremely high temperatures (Brundel and  
314 Arndt, 2016, Russo *et al.*, 2016), potentially related to land-atmosphere feedback processes  
315 (e.g. Seneviratne *et al.*, 2010), through reduced vegetation and soil moisture, perhaps persisting  
316 from 2014-15. Uncertainty in the strength of land-atmosphere coupling over SA remains high  
317 with contradictory results from model analyses (e.g. Koster *et al.*, 2006) and combined  
318 observation-model analysis (Ferguson *et al.*, 2012), suggesting weak and strong coupling,  
319 respectively. Further, warming across SA in recent decades can be attributed substantially to  
320 anthropogenic radiative forcing (Bindoff *et al.*, 2013). As such climate risks are changing. We  
321 estimate that the risk of a 2015-16 magnitude SPEI-7 drought over SA to have increased by  
322 approximately two times due to the effects purely of anthropogenic warming. Note this  
323 estimate does not include any anthropogenic changes in any of the other climate variables  
324 which determine SPEI, most notably precipitation, nor changes in variability of climate (see  
325 Supplementary Information S2). Further, other drought indices may have differing sensitivities  
326 to anthropogenic temperature trends.

327

328 Over the EASE domain as a whole, the 2015-16 event was wet but not extreme, with an SPEI-  
329 7 IAF curve estimated return period (Fig. 3(b)) of only ~10 years (range 5-12 years). The  
330 anomalies were far weaker than that during the 1997-98 El Niño (Fig. 3b). These differences  
331 may be associated with the state of the Indian Ocean Zonal Model (IOZM), an east-west  
332 structure of coupled ocean-atmosphere circulation, influencing convection and rainfall over  
333 East Africa (Saji *et al.*, 1999, Supplementary Information S1). The 1997-98 El Niño coincided  
334 with a very strong positive IOZM event, unlike that of 2015-16, in which the IOZM was weakly  
335 positive. Indeed, the wettest EASE year on record, 1961-1962, experienced a very strongly  
336 positive IOZM event but no El Niño event (Nicholson, 2015).

337

### 338 3.2 Impact of 2015-16 climate anomalies on groundwater storage

339

#### 340 *3.2.1 Large-scale estimates of $\Delta TWS$ , $\Delta SMS$ , $\Delta SWS$ and $\Delta GWS$*

341

342 Regionally, GRACE ensemble-mean  $\Delta TWS$  anomalies (Fig. 4(a)), and estimated  $\Delta GWS$  (eq.  
343 1, Fig. 4(d)), for 2015-16 reflect the north-south dipole over EASE/SA associated with the El  
344 Niño-related SPEI-7 climate anomalies (Fig. 1(a)). Positive  $\Delta TWS$  and  $\Delta GWS$  anomalies exist

345 north of  $\sim 10^\circ\text{S}$  across EASE (including the Makutapora site), the central DRC and northern  
346 Angola. Negative  $\Delta\text{TWS}$  and  $\Delta\text{GWS}$  anomalies occur over an extensive region of eastern SA  
347 including the Limpopo site. However, despite broad-scale structural similarity, there are some  
348 apparent inconsistencies between  $\Delta\text{TWS}$  (and other components of the water budget, including  
349  $\Delta\text{GWS}$ ) and the SPEI-7 climate signal that we consider below.

350

351 Viewed more closely, the partitioning of large-scale  $\Delta\text{TWS}$  anomalies between the modelled  
352  $\Delta\text{SMS}$ ,  $\Delta\text{SWS}$  and residual  $\Delta\text{GWS}$  is spatially complex. First, we note that  $\Delta\text{SWS}$  (Fig. 4(c))  
353 plays only a minor role across the domain. Further, the coherence of the spatial structure in  
354 anomalies in  $\Delta\text{SMS}$  (Fig. 4(b)) is much less clear than for  $\Delta\text{TWS}$ , reflecting uncertainties in  
355 soil moisture among individual LSMs, as highlighted by Scanlon *et al.* (2018). Then,  
356 considering the drought region over SA, a number of features emerge. (i) The relative  
357 magnitude of  $\Delta\text{TWS}$  deficits over South Africa are less than those of the SPEI-7, compared to  
358 the northern more humid parts of SA (compare Figs 4(a) and 1(a)). This difference may be  
359 expected since  $\Delta\text{TWS}$  is an absolute measure of water volume whereas SPEI-7 is a standardised  
360 anomaly relative to climate, derived over a much longer time period from a different rainfall  
361 data than that used in the GLDAS system. Consequently, these measures may be expected to  
362 diverge across mean rainfall gradients. Further, SPEI-7 reflects potential rather than actual  
363 evapotranspiration. (ii) Over the northern sector of Zambia, Zimbabwe and Malawi the strongly  
364 negative  $\Delta\text{TWS}$  anomaly is almost equally shared between modelled reductions in  $\Delta\text{SMS}$  and  
365  $\Delta\text{GWS}$ . (iii) To the south over South Africa however, the (rather weaker)  $\Delta\text{TWS}$  deficits are  
366 effectively accounted for by  $\Delta\text{SMS}$  anomalies such that  $\Delta\text{GWS}$  anomalies are actually close to  
367 zero or indeed slightly positive. The Limpopo study site lies at a transition zone between  
368 regions with apparently strongly reduced  $\Delta\text{GWS}$  to the northeast and close to zero or slightly  
369 positive  $\Delta\text{GWS}$  to the southwest. As geology is broadly continuous across the region, the  
370 transition is largely related to uncertainty in the estimation of modelled  $\Delta\text{SMS}$ .

371

372 Further, considering the anomalous wet region over EASE to the north of  $\sim 10^\circ\text{S}$ ,  $\Delta\text{GWS}$   
373 broadly mirrors the structure of  $\Delta\text{TWS}$ , but the detailed picture is complex. Over most of  
374 Tanzania and Angola positive  $\Delta\text{TWS}$  anomalies are largely partitioned into the  $\Delta\text{GWS}$  rather  
375 than  $\Delta\text{SMS}$ , whereas over southern DRC the reverse is the case. Moreover, there are interesting  
376 apparent contradictions between the climate SPEI-7 and GRACE  $\Delta\text{TWS}$  data. Over Namibia



377 and southern Angola, negative SPEI-7 (Fig. 1(a) and  $\Delta$ SMS, Fig. 4(b)) coincides with positive  
378  $\Delta$ TWS anomalies (Fig. 4(a)) leading to very strong positive  $\Delta$ GWS anomalies (Fig. 4(d)) that  
379 are therefore inconsistent with climate anomalies from SPEI-7. Conversely, and more locally,  
380 over northern Mozambique, a positive  $\Delta$ SMS anomaly, resulting from the driving rainfall data  
381 (see the SPEI-7 wet anomaly, Fig. 1(a)) is not reflected in a strong  $\Delta$ TWS signal, which leaves  
382 a counterintuitive, negative residual response in  $\Delta$ GWS. As such, GRACE  $\Delta$ GWS exhibits  
383 inconsistent responses to both apparent anomalous dry and wet conditions. These are likely to  
384 be a result of (i) limitations in observational precipitation data, (ii) uncertainties in GRACE  
385 TWS retrievals (as well as unwanted artefacts from surface and tectonic deformation) (iii)  
386 uncertainties in estimation the individual components of water storage from LSMs, and (iv)  
387 differing timescales of response across the various data. Such issues have been noted and  
388 assessed elsewhere (Hassan and Jin, 2016; Zhao *et al.*, 2017; Rodell *et al.*, 2018; Scanlon *et*  
389 *al.*, 2018). Resolving these issues is challenging but recent studies have sought to constrain  
390 the uncertainty in the modelled components of water storage through assimilation of GRACE  
391 TWS into hydrological models (Khaki *et al.*, 2018; Schumacher *et al.*, 2018).

392

### 393 3.2.2 *In situ and GRACE-derived estimates of $\Delta$ GWS at the Makutapora and Limpopo Basins*

394

395 Piezometry for the two observatory sites and changes in GWS estimated from GRACE and  
396 LSMs are shown in Fig. 5. First, we note that uncertainty in the mean GRACE  $\Delta$ GWS estimate  
397 (blue shading around blue line in Figs. 5(a) and 5(b)), whilst often large, is generally smaller  
398 than the signals of inter-annual variability which are the main focus of our analysis. However,  
399 variability in mean GRACE  $\Delta$ GWS within recharge seasons is small relative to uncertainty,  
400 such that we cannot confidently draw inferences at these timescales.

401

402 Specifically, at the SA Limpopo site, observed piezometry (Fig. 5(a)) shows an annual cycle  
403 in GWS in most years with a ‘saw tooth’ pattern representing steady recessions in GWS during  
404 the dry season from May to October followed by rapid increases typically starting in December  
405 in response to the onset of the wet season to peak post-wet season in April (lagging peak rainfall  
406 by ~1-2 months). GWS in 2015-16 is well below average with a seasonal but subdued GWS  
407 rise delayed (until March) due to the highly anomalous early wet season drought. The GWS  
408 rise in March-April following rains in March is the second smallest on record; only 2002-3 has

409 lower seasonal increase in GWS. The 2015-16 drought is preceded by negligible recharge in  
410 the dry year of 2014-15 (Fig. 5(a)), such that GWS as of mid-2016 was lowest in the 14-year  
411 record. As such, the major drought of 2015-16 compounded weak recharge in the previous year  
412 to leave GWS at historically low levels. This may have been compounded by increased  
413 abstractions during these dry years.

414

415 Comparison of piezometry and GRACE-derived GWS at Limpopo (Fig 5(a)) suggests a broad  
416 correspondence when seasonally averaged, ( $r = 0.62$ , significant at the 0.01 probability level).  
417 The prolonged decline over 2014-16 is observed in both GRACE and piezometry. When  
418 averaged over all years, the mean annual cycle is similar in phase and magnitude (not shown).  
419 As such, at least broad temporal averaging scales GRACE is corroborated by piezometry at the  
420 Limpopo site, where the scales of spatial averaging are similar. However, within-seasons, the  
421 uncertainty in GRACE  $\Delta$ GWS leads to a much ‘noisier’ mean signal at Limpopo which cannot  
422 resolve the annual ‘saw-tooth’ pattern (Fig. 5(a)): in GRACE  $\Delta$ GWS individual years have a  
423 rather variable annual cycle despite a clear cycle in rainfall. Notably, a strong rise in the  
424 ensemble mean GRACE  $\Delta$ GWS during early season 2015-16 is not corroborated by piezometry  
425 or rainfall. This period coincides with the greatest uncertainty in GRACE  $\Delta$ GWS among the  
426 three GRACE products (see blue shading around ensemble mean GRACE estimates in Fig 5a).  
427 There is some indication from Fig. S2, that during such periods of greatest  $\Delta$ GWS uncertainty,  
428 it is the uncertainty in GRACE  $\Delta$ TWS that makes most important contribution, rather than  
429 uncertainty in the GLDAS components. From the individual GRACE  $\Delta$ TWS products (Fig.  
430 S3) we note that the mean GRACE vs. piezometry  $\Delta$ GWS discrepancies in late 2015 result  
431 largely from the GRGS product, which shows a non-corroborated increase in  $\Delta$ TWS.

432

433 At the EASE Makutapora site, observed piezometric-GWS (Fig. 5(b)) shows little regular inter-  
434 annual variability, with long periods of GWS recessions e.g. 2002-6, 2012-16, interrupted by  
435 irregular and infrequent GWS increases, in declining order of magnitude 2006-7, 2009-10 and  
436 2015-16, all El Niño years. The wet conditions in 2015-16 produced a major recharge event  
437 though observed piezometric responses are smaller than in 2006-7 and 2009-10, despite higher  
438 rainfall (Fig. 5(b)). Under highly dynamic pumping regimes (Fig. 5(c)), GWS changes are only  
439 a partial proxy for groundwater recharge; the sharp increase (~50%) in wellfield pumping in  
440 May 2015 served to diminish the response in piezometric-GWS to the 2015-16 El Niño.

441 Overall, however, the findings are consistent with the analysis of Taylor *et al.* (2013) who note  
442 highly episodic recharge at Makutapora over the period since the 1960s associated with years  
443 of heavy rainfall. The 2015-16 El Niño event represents a major event driving GWS at the  
444 Makutapora wellfield, despite moderate rainfall anomalies over EASE.

445

446 There is only a rather general association between GRACE and piezometric estimates of  
447 groundwater storage variability at the Makutapora site. However, the episodic recharge events  
448 in the piezometry data of 2006-7, 2009-10 and 2015-16 are matched quite well by the  
449 magnitude of major GRACE increases in  $\Delta$ GWS, although the second largest GRACE  $\Delta$ GWS  
450 increase occurs in 2014-15 with no response apparent in piezometry. Overall, the seasonal  
451 correlation of GRACE  $\Delta$ GWS and piezometric GWS of 0.51 is only moderate (significant at  
452 the 0.05 probability level) but clearly reflects the low frequency multi-annual trends (at least  
453 up to 2013) as well as interannual variability.

454

455 However, stark differences between GRACE and piezometry are apparent. In contrast to  
456 piezometry, GRACE (Fig. 5(b)) shows increases in  $\Delta$ GWS in almost every year (with lag of  
457  $\sim$ 1 month after the rainfall annual peak), suggesting recharge occurs annually, in contrast to  
458 the piezometry. Further, GRACE  $\Delta$ GWS replicates the low frequency recessionary trend over  
459 the period 2002-07 but not since 2012. Resolving these contradictions is problematic but two  
460 likely explanations emerge (i) Incommensurate scales of observation from piezometry (area  
461  $\sim$ 60 km<sup>2</sup>) and GRACE ( $\sim$ 200,000 km<sup>2</sup>). More localised processes may dominate the piezometry  
462 record, perhaps including recharge sensitivity to contributions from local ephemeral river flow  
463 and rainfall. Further, the effects of local pumping strongly influence the piezometric record,  
464 obscuring recharge events of low magnitude. This could explain the discrepancies in low  
465 frequency trends between the GRACE and piezometry. Specifically, the period 2002-07 over  
466 the which the data agree reflects a widespread groundwater recession, following the  
467 anomalously high recharge during the El Niño event of 1997-98 (Taylor *et al.*, 2013), whilst  
468 the recent accelerated recessionary trend since 2012 reflects the effects of a rapid increase in  
469 abstraction, which has a more localised effect apparent only in the piezometric observations.  
470 As such the piezometric record may only show episodic recharge whilst GRACE may indicate  
471 annual and episodic recharge processes. (ii) Errors in GRACE  $\Delta$ GWS resulting from inaccurate  
472 accounting of  $\Delta$ SMS and  $\Delta$ SWS, which leaves a residual artefact of an annual positive  $\Delta$ GWS

473 signal, see Section 3.1, *Shamsudduha et al.* (2017) and *Scanlon et al.* (2018). Such errors may  
474 not be adequately accounted for in the uncertainty estimates in GRACE  $\Delta$ GWS given, for  
475 example similarities in LSM design and driving data. Indeed, at both the Limpopo and  
476 Makutapora sites, we note stronger correlations between seasonal local rainfall and piezometric  
477 GWS than with GRACE  $\Delta$ GWS (not shown).

478

#### 479 **4. Concluding Discussion**

480

481 We quantify the climate anomalies and groundwater response during the major El Niño event  
482 of 2015-16, over Southern and Eastern Africa, south of the equator, across a range of spatial  
483 scales from regional to local. Our analysis confirms that the event was associated with a  
484 pronounced north/south dipole pattern of positive/negative rainfall and water balance  
485 anomalies over EASE/SA, typical of the ENSO teleconnection to the region. It was the second  
486 largest such dipole event on record since 1900. Considerable diversity nevertheless exists in  
487 climate anomalies over Africa between El Niño events.

488

489 The response of the water balance including GWS to ENSO is marked. Over EASE, total  
490 rainfall and daily intensities were higher than normal and we estimate the return period for the  
491 SPEI-7 water balance metric, over the domain as a whole, to be ~10 years. Wet anomalies over  
492 EASE were actually moderated by the occurrence of a rather weak IOZM event. Nevertheless,  
493 the anomalously wet conditions led to strong groundwater recharge over the EASE domain as  
494 evidenced from GRACE. At the Makutapora wellfield in Tanzania, 2015-16 the strong El  
495 Niño-related rainfall acted to reverse a long-term decline in observed in-situ groundwater  
496 storage associated with a rise in intensive pumping rates. Changes in GWS estimated from an  
497 ensemble of GRACE and LSMs also reflect the occurrence of substantial groundwater recharge  
498 in 2015-16 and indicate annual groundwater recharge across the region. Broadly, the analysis  
499 reinforces the importance of large-scale climate events in driving episodic recharge, critical to  
500 replenish heavily exploited aquifers.

501

502 Over SA, the 2015-16 El Niño was associated with extreme drought, the strongest within the  
503 observed 116-year record, with an estimated return period of ~260 years, resulting from  
504 exceptionally low rainfall and high temperatures. The drought resulted in groundwater storage

505 declines through most of the wet season at our Limpopo study site, with strongly reduced  
506 recharge experienced, the second lowest on record. Furthermore, this followed a dry year 2014-  
507 15 leading to two consecutive years of low recharge and the greatest recession on record.  
508 Clearly, groundwater provides a valuable buffer for periods of reduced surface water  
509 availability in drought conditions, although as our results at Limpopo show, consecutive dry  
510 years lead to marked storage reduction. Climate projections suggest reduced early season  
511 rainfall across much of SA (Lazenby *et al.* 2018) compounding rising temperatures, and the  
512 implications of this for climate resilience require a better understanding of these impacts on  
513 groundwater recharge as well as surface water resources.

514

515 GRACE data and LSM outputs are clearly useful in complementing in-situ data, but a number  
516 of issues emerge. Although at the broadest scale the GRACE  $\Delta$ GWS anomalies in 2015-16 are  
517 consistent with rainfall anomalies, there are a number of apparent inconsistencies over quite  
518 large areas. Resolving the underlying reasons for these is problematic, but likely candidates  
519 include the effects of inadequate climate data over Southern Africa, influencing and  
520 compounded by uncertainties in  $\Delta$ SMS and  $\Delta$ SWS estimates simulated by land surface models,  
521 on which the estimation of GRACE  $\Delta$ GWS depends. When averaged over comparable scales  
522 at Limpopo GRACE and piezometry agree well, at least for seasonal averages. Comparison  
523 with the local observations shows that GRACE GWS estimates are considerably noisier,  
524 especially at Makutapora where the spatial averaging scale of in-situ data and GRACE differ  
525 greatly. Local groundwater abstractions are apparent in the Makutapora record and very likely  
526 at Limpopo. Our results suggest that further analysis of the robustness of GRACE estimates of  
527 GWS is advisable and, as such, these estimates should be treated with considerable caution.

528

529 Our results highlight the potential for adaptive strategies, such as managed aquifer recharge,  
530 for optimising the capture or storage of episodic recharge in East Africa during El Niño and/or  
531 positive IOZM events, and by corollary over Southern Africa during La Niña events (given the  
532 opposing dipole structure of ENSO-related rainfall anomalies across SA/EASE). Of course  
533 other modes of climate variability driving rainfall extremes are also important. Such  
534 interventions can enhance the positive role of groundwater in climate-resilient water and  
535 drought management. Seasonal climate prediction may have a potential role to inform such  
536 adaptive water management strategies. At Makutapora, managed aquifer recharge exploiting

537 El Niño and/or positive IOZM events may contribute to resilient urban water supply systems  
538 for the city of Dodoma. Our findings strengthen the case for a greater understanding of the  
539 drivers of rainfall extremes over Africa and their relationship with recharge processes under  
540 past, current and future climates and at various temporal and spatial scales. Such knowledge is  
541 crucial to inform water management policies and practices for sustainable and climate resilient  
542 development in a region undergoing rapid development of groundwater resources.

543

544 **Competing Interests.** The authors confirm they have no competing interests

545

546 **Author contribution.** SK and MT conceived the paper. Data analysis was conducted by all  
547 authors. MT and SK prepared the manuscript with contributions from all co-authors.

548

#### 549 **Acknowledgements**

550

551 This project was supported by the following research grant awards, funded by the UK Natural  
552 Environment Research Council (NERC) and Economic and Social Research Council (ESRC)  
553 and the UK Department for International Development (DfID): (i) The Unlocking the Potential  
554 of Groundwater for Poverty Alleviation (UpGro) consortium project ‘*GroFutures*’ Grant  
555 numbers NE/M008207/1 and NE/M008932/1; see [www.grofutures.org](http://www.grofutures.org)) (ii) The Future  
556 Climate For Africa (FCFA) consortium project ‘UMFULA’ grant number NE/M020258 (see  
557 [www.futureclimateafrica.org](http://www.futureclimateafrica.org)) (iii) The Science for Humanitarian Emergencies And Resilience  
558 (SHEAR) consortium project ‘ForPac’ Grant number NE/P000673/1 and NE/P000568/1 (see  
559 [www.forpac.org](http://www.forpac.org)). Further contribution was received from the UK Engineering and Physical  
560 Sciences Research Council (EPSRC) ‘Banking the Rain’ grant number 172313 under the  
561 Global Challenges Research Fund (GCRF), and The Royal Society Leverhulme Senior  
562 Fellowship to RT (Ref. LT170004). MOC is supported by a UK NERC Independent Research  
563 Fellowship, grant number NE/P017819/1. *The Chronicles Consortium* (<https://www.un-igrac.org/special-project/chronicles-consortium>), which coordinates long-term groundwater in  
564 situ observations was supported by the UK government under the UPGro programme. This  
565 research used science gateway resources of the National Energy Research Scientific  
566 Computing Center, a DOE Office of Science User Facility supported by the Office of Science  
567 of the U.S. Department of Energy under Contract No. DE-AC02-05CH11231. The authors

569 would like to thank the Editor and reviewers for their constructive comments and suggestions  
570 which led to substantial improvements in the manuscript.  
571



572 **References**

573

574 Archer, E. R. M., Landman, W. A., Tadross, M. A., Malherbe, J., Weepener, H., Maluleke, P.,  
575 & Marumbwa, F. M.: Understanding the evolution of the 2014–2016 summer rainfall seasons  
576 in southern Africa: Key lessons, *Clim. Risk Manag.*, 16, 22-28, 2017.

577

578 Biancale, R., Lemoine, J-M., Balmino, G., Loyer, S., Bruisma, S., Perosanz, .F, Marty, J-C.,  
579 and Gégout, P.: 3 Years of Geoid Variations from GRACE and LAGEOS Data at 10-day  
580 Intervals from July 2002 to March 2005, CNES/GRGS, 2006

581

582 Bindoff, N.L., P.A. Stott, K.M. AchutaRao, M.R. Allen, N. Gillett, D. Gutzler, K. Hansingo,  
583 G. Hegerl, Y. Hu, S. Jain, I.I. Mokhov, J. Overland, J. Perlwitz, R. Sebbari and X. Zhang,:  
584 Detection and Attribution of Climate Change: from Global to Regional. In: Climate Change  
585 2013: The Physical Science Basis. Contribution of Working Group I to the Fifth Assessment  
586 Report of the Intergovernmental Panel on Climate Change [Stocker, T.F., D. Qin, G.-K.  
587 Plattner, M. Tignor, S.K. Allen, J. Boschung, A. Nauels, Y. Xia, V. Bex and P.M. Midgley  
588 (eds.)]. Cambridge University Press, Cambridge, United Kingdom and New York, NY, USA,  
589 2013.

590

591 Berhane, F., & Zaitchik, B: Modulation of daily precipitation over East Africa by the Madden–  
592 Julian oscillation, *J. Climate*, 27(15), 6016-6034, 2014.

593

594 Blamey, R. C., Kolusu, S. R., Mahlalela, P., Todd, M. C., & Reason, C. J. C: The role of  
595 regional circulation features in regulating El Niño climate impacts over southern Africa: A  
596 comparison of the 2015/2016 drought with previous events, *Int. Journal of Climatol.*,  
597 <https://doi.org/10.1002/joc.5668>, 2018.

598

599 Blunden, J., & Arndt, D. S. : State of the Climate in 2016, *B. Amer. Met. Soc.*, 98(8), Si-S280,  
600 2016.

601

602 Bonsor, H., Shamsudduha, M., Marchant, B., MacDonald, A., & Taylor, R: Seasonal and  
603 decadal groundwater changes in African sedimentary aquifers estimated using GRACE  
604 products and LSMs, *Remote Sens.*, 10(6), 904, 2018.

605 Cai, X., Magidi, J., Nhamo, L., & van Koppen, B.: *Mapping irrigated areas in the Limpopo*  
606 *Province, South Africa*(Vol. 172),International Water Management Institute (IWMI Working  
607 Paper 172), doi: 10.5337/2017.205, 2017.

608 Calow, R. C., MacDonald, A. M., Nicol, A. L., & Robins, N. S. : Ground water security and  
609 drought in Africa: linking availability, access, and demand, *Groundwater*, 48(2), 246-256,  
610 2010.

611

612 Cuthbert, M. O., Acworth, R. I., Andersen, M. S., Larsen, J. R., McCallum, A. M., Rau, G. C.,  
613 & Tellam, J. H.: Understanding and quantifying focused, indirect groundwater recharge from  
614 ephemeral streams using water table fluctuations, *Water Resour. Res.*, 52(2), 827-840,  
615 doi:10.1002/2015WR017503, 2016.

616

617 Cuthbert, M. O., Gleeson, T., Reynolds, S. C., Bennett, M. R., Newton, A. C., McCormack, C.  
618 J., & Ashley, G. M. : Modelling the role of groundwater hydro-refugia in East African hominin  
619 evolution and dispersal, *Nature Com.*, 8, 15696, 2017.

620

621 Dai, Y., Zeng, X., Dickinson, R. E., Baker, I., Bonan, G. B., Bosilovich, M. G., ... & Oleson,  
622 K. W. :The common land model, *B. Amer. Met. Soc.*, 84(8), 1013-1024, 2003.

623

624 Dee, D. P., Uppala, S. M., Simmons, A. J., Berrisford, P., Poli, P., Kobayashi, S., ... & Bechtold,  
625 P.: The ERA-Interim reanalysis: Configuration and performance of the data assimilation  
626 system, *Q. J. Roy. Meteor. Soc.*, 137(656), 553-597, 2011.

627

628 Dunning, C. M., Black, E. C., & Allan, R. P. : The onset and cessation of seasonal rainfall over  
629 Africa, *J. Geophys. Res.-Atmos.*, 121(19), 2016.

630

631 Ek, M. B., Mitchell, K. E., Lin, Y., Rogers, E., Grunmann, P., Koren, V., ... & Tarpley, J. D.  
632 :Implementation of Noah land surface model advances in the National Centers for

633 Environmental Prediction operational mesoscale Eta model, *J. Geophys. Res.-*  
634 *Atmos.*, 108(D22), 2003.

635

636 Ferguson, C. R., Wood, E. F., & Vinukollu, R. K. : A global intercomparison of modeled and  
637 observed land–atmosphere coupling, *J. Hydromet.*, 13(3), 749-784, 2012.

638

639 Harris, I. P. D. J., Jones, P. D., Osborn, T. J., & Lister, D. H. :Updated high-resolution grids of  
640 monthly climatic observations–the CRU TS3. 10 Dataset, *Int. J. Climatol.*, 34(3), 623-642,  
641 2014.

642

643 Hassan, A., & Jin, S.: Water storage changes and balances in Africa observed by GRACE and  
644 hydrologic models, *Geo. Geody.*, 7 (1), 39-49. <https://doi.org/10.1016/j.geog.2016.03.002>,  
645 2016

646

647

648 Holman, I. P., Rivas-Casado, M., Bloomfield, J. P., & Gurdak, J. J. : Identifying non-stationary  
649 groundwater level response to North Atlantic ocean–atmosphere teleconnection patterns using  
650 wavelet coherence, *Hydrogeol. Jour.*, 19(6), 1269, 2011.

651

652 Hunter, P. R., MacDonald, A. M., & Carter, R. C. : Water supply and health, *PLoS*  
653 *Medicine*, 7(11), e1000361, <https://doi.org/10.1371/journal.pmed.1000361>, 2010.

654

655 Jasechko, S., & Taylor, R. G. : Intensive rainfall recharges tropical groundwaters. *Env.*  
656 *Research Let.*, 10(12), 124015, doi:10.1088/1748-9326/10/12/124015, 2015.

657

658 Khaki, M., Forootan, E., Kuhn, M., Awange, J., van Dijk, A.I.J.M., Schumacher, M., & Sharifi,  
659 M.A. Determining Water Storage Depletion within Iran by Assimilating GRACE data into the  
660 W3RA Hydrological Model, *Adv. Water Resour.*, doi: 10.1016/j.advwatres.2018.02.008, 2018

661

662 Koster, R. D., & Suarez, M. J. :Modeling the land surface boundary in climate models as a  
663 composite of independent vegetation stands, *J. Geophys. Res.-Atmos.*, , 97(D3), 2697-2715,  
664 1992.

665

666 Koster, R. D., Sud, Y. C., Guo, Z., Dirmeyer, P. A., Bonan, G., Oleson, K. W., ... & Kowalczyk,  
667 E. : GLACE: the global land-atmosphere coupling experiment. Part I: overview, *J.*  
668 *Hydromet.*, 7(4), 590-610, 2006.

669

670 Kuss, A. J. M., & Gurdak, J. J. : Groundwater level response in US principal aquifers to ENSO,  
671 NAO, PDO, and AMO, *J. Hydro.*, 519, 1939-1952, 2014.

672

673 Landerer, F. W., & Swenson, S. C. :Accuracy of scaled GRACE terrestrial water storage  
674 estimates, *Water Resour. Res.*, 48(4), 2012.

675

676 Lazenby, M. J., Todd, M. C., & Wang, Y., Chadwick. R.:Future precipitation projections over  
677 central and southern Africa and the adjacent Indian Ocean: What causes the changes and the  
678 uncertainty? *J. Climate*, 31, 4807-4826, 2018

679

680 Liang, X., Xie, Z., & Huang, M. :A new parameterization for surface and groundwater  
681 interactions and its impact on water budgets with the variable infiltration capacity (VIC) land  
682 surface model, *J. Geophys. Res.-Atmos.*, 108(D16), 2003.

683

684 MacDonald, A. M., Bonsor, H. C., Dochartaigh, B. É. Ó., & Taylor, R. G. :Quantitative maps  
685 of groundwater resources in Africa, *Env. Research Let.*, 7(2), 024009, 2012.

686

687 McMahon, T. A., Finlayson, B. L., Haines, A., & Srikanthan, R.: Runoff variability: a global  
688 perspective, In *The Influence of Climate Change and Climatic Variability on the Hydrologic*  
689 *Regime and Water Resources*, Proceedings of the Vancouver Symposium, August 1987. IAHS  
690 Publ. no. 168, 1987.

691

692 Meyer, R.: Analysis of groundwater level time series and the relation to rainfall and recharge,  
693 Water Resources Commission (South Africa), report number 1323/1/05, 2005.

694

695 Mishra, V., & Cherkauer, K. A.: Retrospective droughts in the crop growing season:  
696 Implications to corn and soybean yield in the Midwestern United States, *Agr. Forest*  
697 *Met.*, 150(7-8), 1030-1045, 2010.

698

699 Nicholson, S.E.: Long-term variability of the East African ‘short rains’ and its links to large-  
700 scale factors, *Int. J. Climatol.*, 35(13), 3979-3990, 2015

701

702 Nicholson, S. E.: Climate and climatic variability of rainfall over eastern Africa, *Reviews of*  
703 *Geophysics*, 55(3), 590-635, 2017.

704

705 Owor, M., Taylor, R. G., Tindimugaya, C., & Mwesigwa, D.: Rainfall intensity and  
706 groundwater recharge: empirical evidence from the Upper Nile Basin, *Env. Research*  
707 *Let.*, 4(3), 035009, 2009.

708

709 Ratnam, J. V., Behera, S. K., Masumoto, Y., & Yamagata, T. :Remote effects of El Niño and  
710 Modoki events on the austral summer precipitation of southern Africa, *J. Climate*, 27(10),  
711 3802-3815, 2014.

712

713 Rodell, M., Houser, P. R., Jambor, U. E. A., Gottschalck, J., Mitchell, K., Meng, C. J., ... &  
714 Entin, J. K. ;The global land data assimilation system, *B. Am. Meteorol.*, 85(3), 381-394, 2004.

715

716 Rodell , M., Famiglietti, S., Wiese, D.N., Reager, J.T., Beaudoing, H. K., Landerer F. W.  
717 & Lo, M.-H. : Emerging trends in global freshwater availability, *Nature*, 557, 651- 659.  
718 <https://www.nature.com/articles/s41586-018-0123-1>, 2018

719

720 Ropelewski, C. F., & Halpert, M. S.: Global and regional scale precipitation patterns associated  
721 with the El Niño/Southern Oscillation, *Mon. Weather Rev.*, 115(8), 1606-1626, 1987.

722

723 Russo, S., Marchese, A. F., Sillmann, J., & Immé, G.: When will unusual heat waves become  
724 normal in a warming Africa?, *Env. Research Let.*, 11(5), 054016, 2016.

725

726 SADC 2016a: SADC regional situation update on El Nino-induced drought, Issue 02, 12th  
727 September 2016, SADC, 12pp, available at:

728 ,[https://www.sadc.int/files/9514/7403/9132/SADC\\_Regional\\_Situation\\_Update\\_No-2\\_16-](https://www.sadc.int/files/9514/7403/9132/SADC_Regional_Situation_Update_No-2_16-)  
729 [09-2016.pdf](https://www.sadc.int/files/9514/7403/9132/SADC_Regional_Situation_Update_No-2_16-09-2016.pdf), 2016.  
730  
731 SADC 2016b: SADC Regional Vulnerability Assessment and Analysis Synthesis Report: State  
732 of Food Insecurity and Vulnerability in the Southern African Development Community,  
733 SADC, 66pp, available at: [https://www.sadc.int/files/9014/7911/5767/SADC\\_RVAA-](https://www.sadc.int/files/9014/7911/5767/SADC_RVAA-August-Final-Web.pdf)  
734 [August-Final-Web.pdf](https://www.sadc.int/files/9014/7911/5767/SADC_RVAA-August-Final-Web.pdf), 2016  
735  
736 Saji, N. H., Goswami, B. N., Vinayachandran, P. N., & Yamagata, T.: A dipole mode in the  
737 tropical Indian Ocean, *Nature*, 401(6751), 360, doi:10.1038/43854, 1999.  
738  
739 Scanlon, B. R., Zhang, Z., Save, H., Sun, A. Y., Schmied, H. M., van Beek, L. P., ... &  
740 Longuevergne, L. : Global models underestimate large decadal declining and rising water  
741 storage trends relative to GRACE satellite data, *P. Natl. Acad. Sci.*, 201704665,  
742 <https://doi.org/10.1073/pnas.1704665115>, 2018.  
743  
744 Schneider, U., Becker, A., Finger, P., Meyer-Christoffer, A., Rudolf, B., Markus, Z.: GPCP  
745 Full Data Reanalysis Version 6.0 at 0.5°: Monthly Land-Surface Precipitation from Rain-  
746 Gauges built on GTS-based and Historic Data. DOI: [10.5676/DWD\\_GPCP/FD\\_M\\_V6\\_100](https://doi.org/10.5676/DWD_GPCP/FD_M_V6_100),  
747 [2011](https://doi.org/10.5676/DWD_GPCP/FD_M_V6_100).  
748  
749 Schneider, U., Becker, A., Finger, P., Meyer-Christoffer, A., Ziese, M., & Rudolf, B. : GPCP's  
750 new land surface precipitation climatology based on quality-controlled in situ data and its role  
751 in quantifying the global water cycle, *Theor. Appl. Climatol.*, 115(1-2), 15-40, 2014.  
752  
753 Schumacher, M., Forootan, E., van Dijk, A.I.J.M., Muller Schmied, H., Crosbie, R.S., Kusche,  
754 855 J., & Dll, P. Improving drought simulations within the Murray-Darling Basin by 856  
755 combined calibration/assimilation of GRACE data into the WaterGAP Global Hydrology 857  
756 Model, *Remote Sens. Environ.*, 204, 212-228, <https://doi.org/10.1016/j.rse.2017.10.029>, 2018  
757

758 Seneviratne, S. I., Corti, T., Davin, E. L., Hirschi, M., Jaeger, E. B., Lehner, I., ... & Teuling,  
759 A. J.: Investigating soil moisture–climate interactions in a changing climate: A review, *Earth*  
760 *Review.*, 99(3-4), 125-161, doi:10.1016/j.earscirev.2010.02.004, 2010.

761

762 Shamsudduha, M., Taylor, R. G., Jones, D., Longuevergne, L., Owor, M., & Tindimugaya, C.  
763 :Recent changes in terrestrial water storage in the Upper Nile Basin: an evaluation of commonly  
764 used gridded GRACE products, *Hydrol. Earth Syst. Sci.*, 21(9), 4533-4549,  
765 <https://doi.org/10.5194/hess-21-4533-2017>, 2017.

766

767 Siderius, C., Gannon, K. E., Ndiyoi, M., Opere, A., Batisani, N., Olago, D., ... & Conway, D.  
768 :Hydrological response and complex impact pathways of the 2015/2016 El Niño in Eastern and  
769 Southern Africa, *Earth's Fut.*, 6(1), doi:10.1002/2017EF000680,2-22, 2018.

770

771 Smith, T. M., Reynolds, R. W., Peterson, T. C., & Lawrimore, J. : Improvements to NOAA's  
772 historical merged land–ocean surface temperature analysis (1880–2006). *J. Climate*, 21(10),  
773 2283-2296, 2008.

774

775 Swenson, S., & Wahr, J.: Post-processing removal of correlated errors in GRACE  
776 data, *Geophys. Res. Lett.*, 33(8), 2006.

777

778 Taylor, R. G., Koussis, A. D., & Tindimugaya, C.: Groundwater and climate in Africa—a  
779 review, *Hydro. Sci. Jour.*, 54(4), 655-664, 2009.

780

781 Taylor, R. G., Todd, M. C., Kongola, L., Maurice, L., Nahozya, E., Sanga, H., & MacDonald,  
782 A. M. : Evidence of the dependence of groundwater resources on extreme rainfall in East  
783 Africa, *Nature Clim. Chan.*, 3(4), 374, 2013.

784

785 van Wyk, E., Van Tonder, G. J., & Vermeulen, D.: Characteristics of local groundwater  
786 recharge cycles in South African semi-arid hard rock terrains–rainwater input, *Water SA*, 37(2),  
787 <http://dx.doi.org/10.4314/wsa.v37i2.65860>, 2011.

788



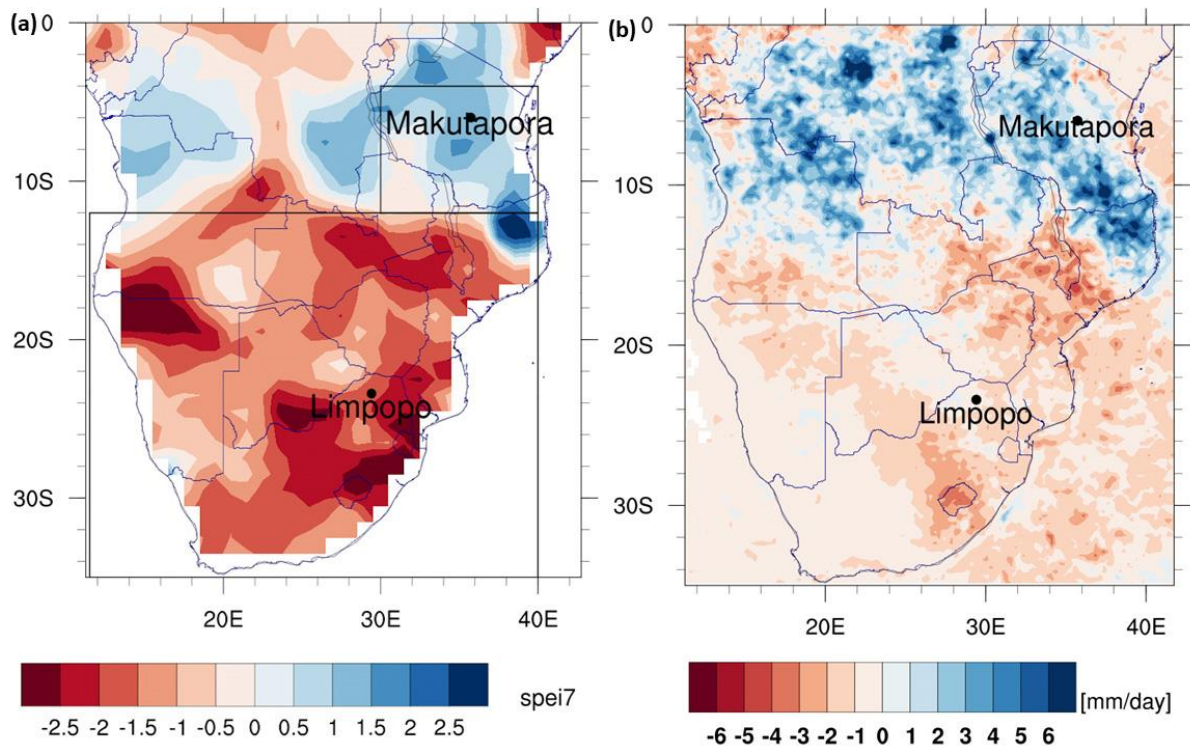
789 Vicente-Serrano, S. M., Beguería, S., & López-Moreno, J. I. : A multiscale drought index  
790 sensitive to global warming: the standardized precipitation evapotranspiration index, *J.*  
791 *Climate*, 23(7), 1696-1718, 2010.  
792

793 Villholth, K. G. : Groundwater irrigation for smallholders in Sub-Saharan Africa—a synthesis  
794 of current knowledge to guide sustainable outcomes, *Water intern.*, 38(4), 369-391, 2013.  
795

796 Watkins, M. M., Wiese, D. N., Yuan, D. N., Boening, C., & Landerer, F. W. : Improved  
797 methods for observing Earth's time variable mass distribution with GRACE using spherical cap  
798 mascons, *J. Geo. Res.: Solid Earth*, 120(4), 2648-2671, 2015.  
799

800 Wiese, D. N., Yuan, D-N., Boening, C., Landerer, F. W., & Watkins, M. M.: JPL GRACE  
801 Mascon Ocean, Ice, and Hydrology Equivalent Water Height, JPL RL05M.1. Ver. 1 PO.DAAC  
802 CA USA, 2015.  
803

804 Zhao, M., Velicogna, G.A.I., & Kimball, J.S.: Satellite observations of regional drought  
805 severity in the continental United States using GRACE-based terrestrial water storage changes,  
806 *J. Climate*, 30, 6297-6308. DOI: 10.1175/JCLI-D-16-0458.1, 2017  
807  
808



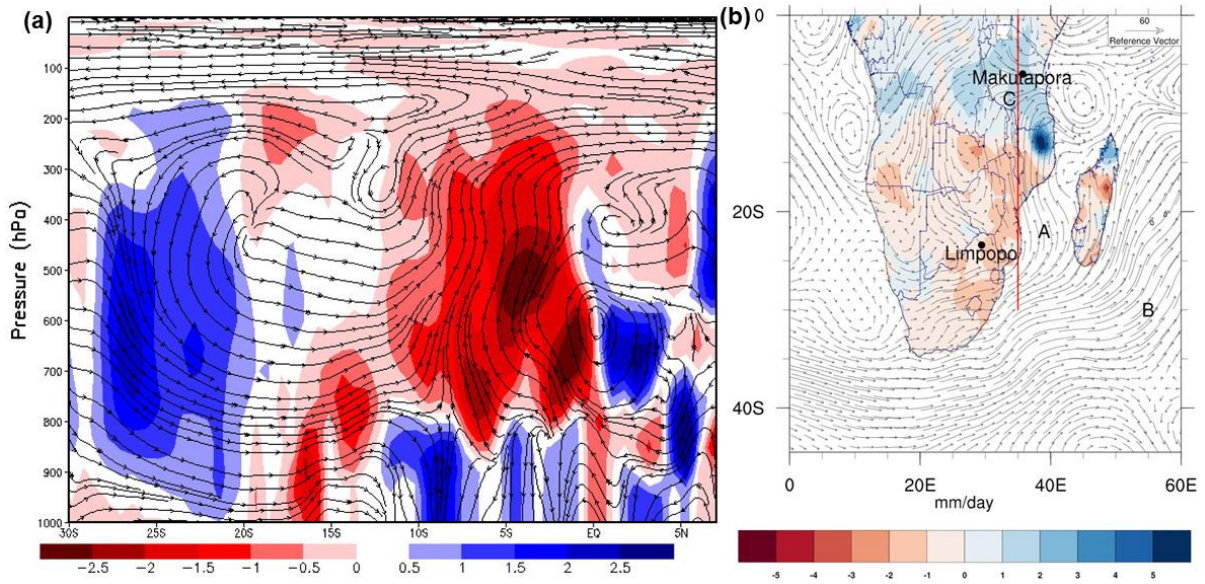
809

810

811 Fig. 1. Large-scale climate anomalies over the study region for October-April 2015-16. (a)  
 812 SPEI-7 (b) Anomalies of the 80th percentile of daily TRMM rainfall ( $\text{mm day}^{-1}$ ). Boxes in (a)  
 813 show the EASE (small box) and SA (large box) domains used in the SPEI-7 IAF analysis (see  
 814 Section 2.1 and S2). The piezometer observation locations are also shown.

815

816

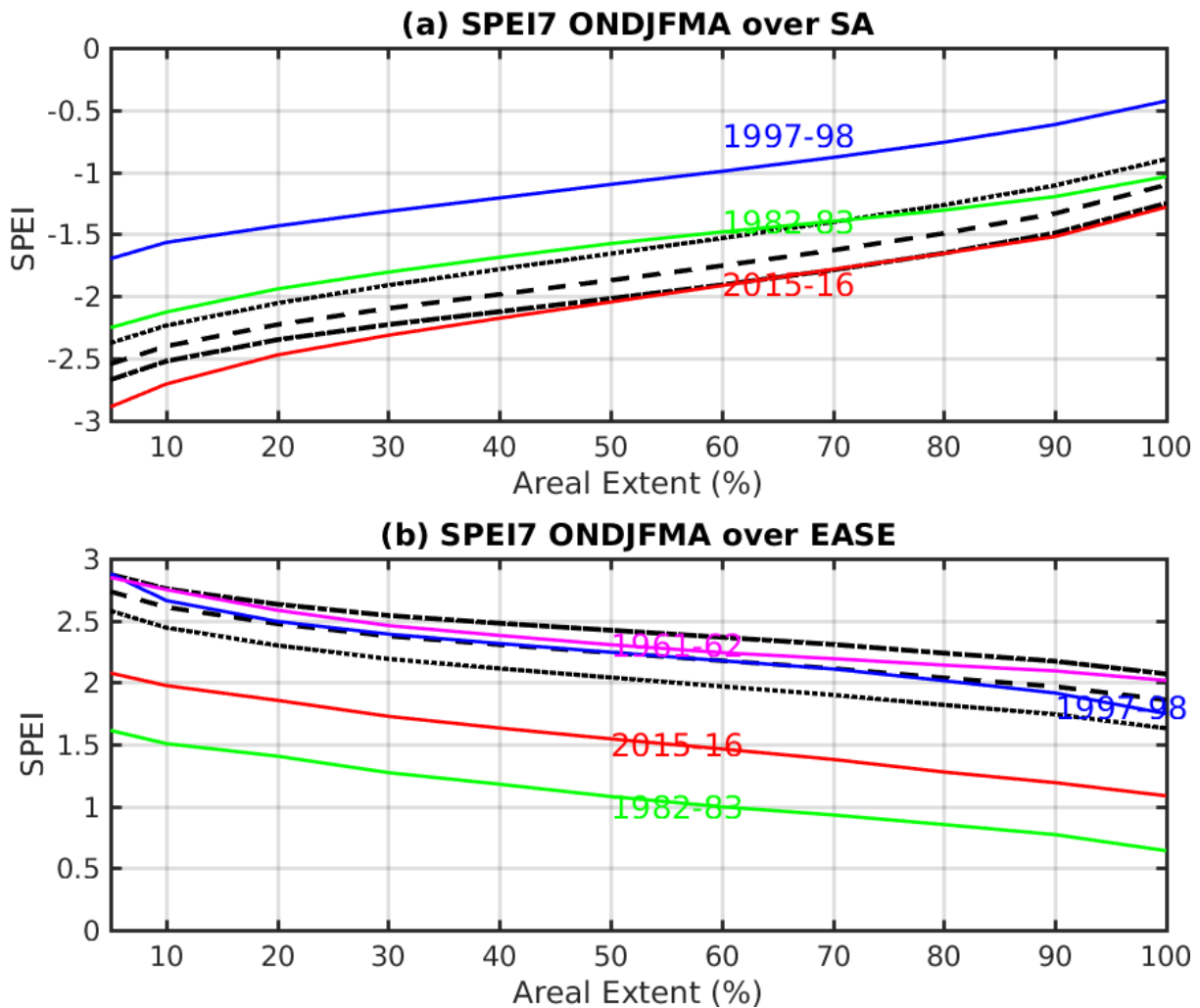


817

818

819

820 Fig. 2. Circulation anomalies for October-April 2015-2016. (a) Latitude-height transect plot of  
 821 anomalous meridional overturning circulation (streamlines of vertical and meridional wind)  
 822 and vertical velocity anomalies ( $\text{m s}^{-1}$ , shaded) averaged over the 35-37°E. This latitude transect  
 823 is shown as a red line on the map in Fig. 2(b). (b) Vertically integrated moisture flux anomalies  
 824 ( $\text{g kg}^{-1} \text{m s}^{-2}$ , vectors) and rainfall anomalies ( $\text{mm day}^{-1}$ , shaded).



825

826

827 Fig. 3. Intensity-Areal extent-Frequency (IAF) curves (See Section 2.1 and Section S2 for  
 828 details of method) estimated from the seasonal mean SPEI-7 (derived with Penman-Monteith  
 829 PET, see text for uncertainty ranges) over (a) the southern Africa domain ( $10.5^{\circ}$ - $35.5^{\circ}$ S, see  
 830 box in Fig. 1a); (b) the east Africa domain  $30^{\circ}$ - $40^{\circ}$ E,  $4^{\circ}$ - $12^{\circ}$ S, see box in Fig. 1a). On the x-  
 831 axis is the areal extent over which the SPEI is averaged and the y-axis is the SPEI-7 drought  
 832 intensity. Solid coloured lines show the IAF curves for the study El Niño event years; 2015-16  
 833 (red), 1997-98 (blue), 1982-83 (green) and (in (b) only) the 1961-62 Indian Ocean Zonal Mode  
 834 event (purple). Black lines are the IAF curves for selected benchmark return periods, from top  
 835 to bottom in (a) (and bottom to top in (b)), 50 years (dotted), 100 years (dashed) and 200 years  
 836 (dot-dashed).

837  
838  
839  
840  
841  
842  
843  
844  
845  
846  
847  
848  
849  
850  
851  
852  
853  
854  
855  
856  
857  
858  
859  
860  
861  
862  
863  
864  
865  
866

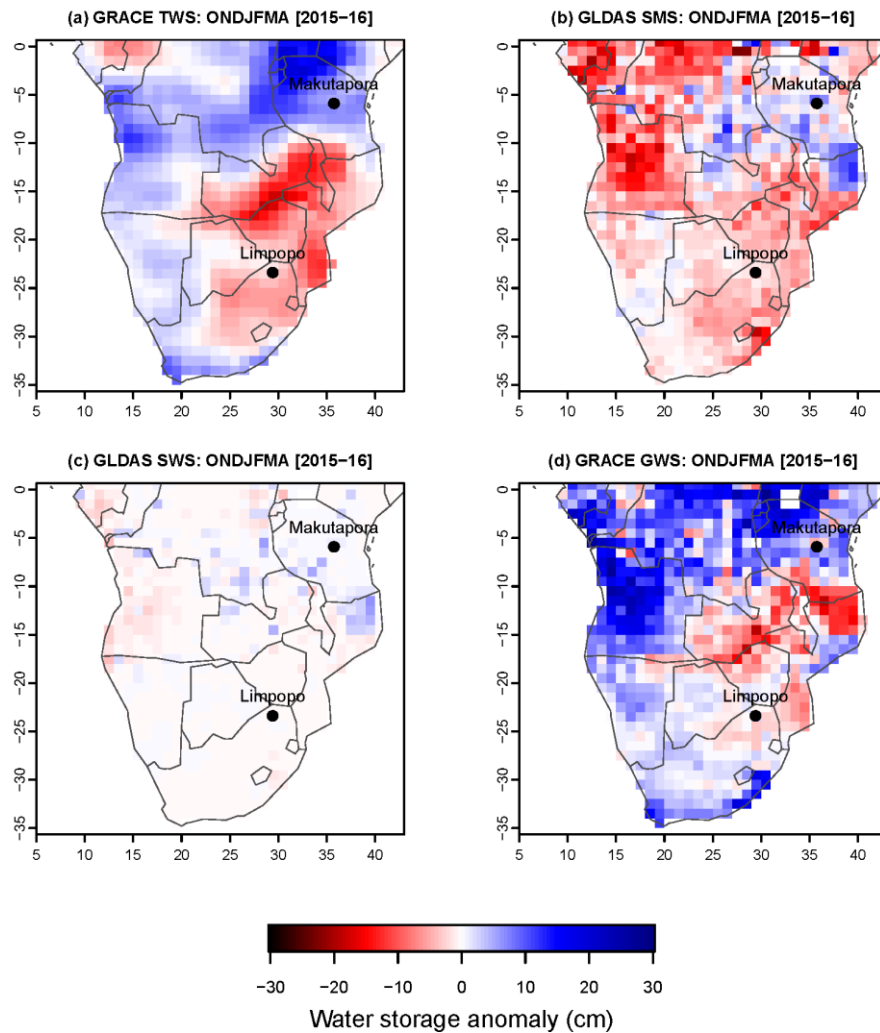
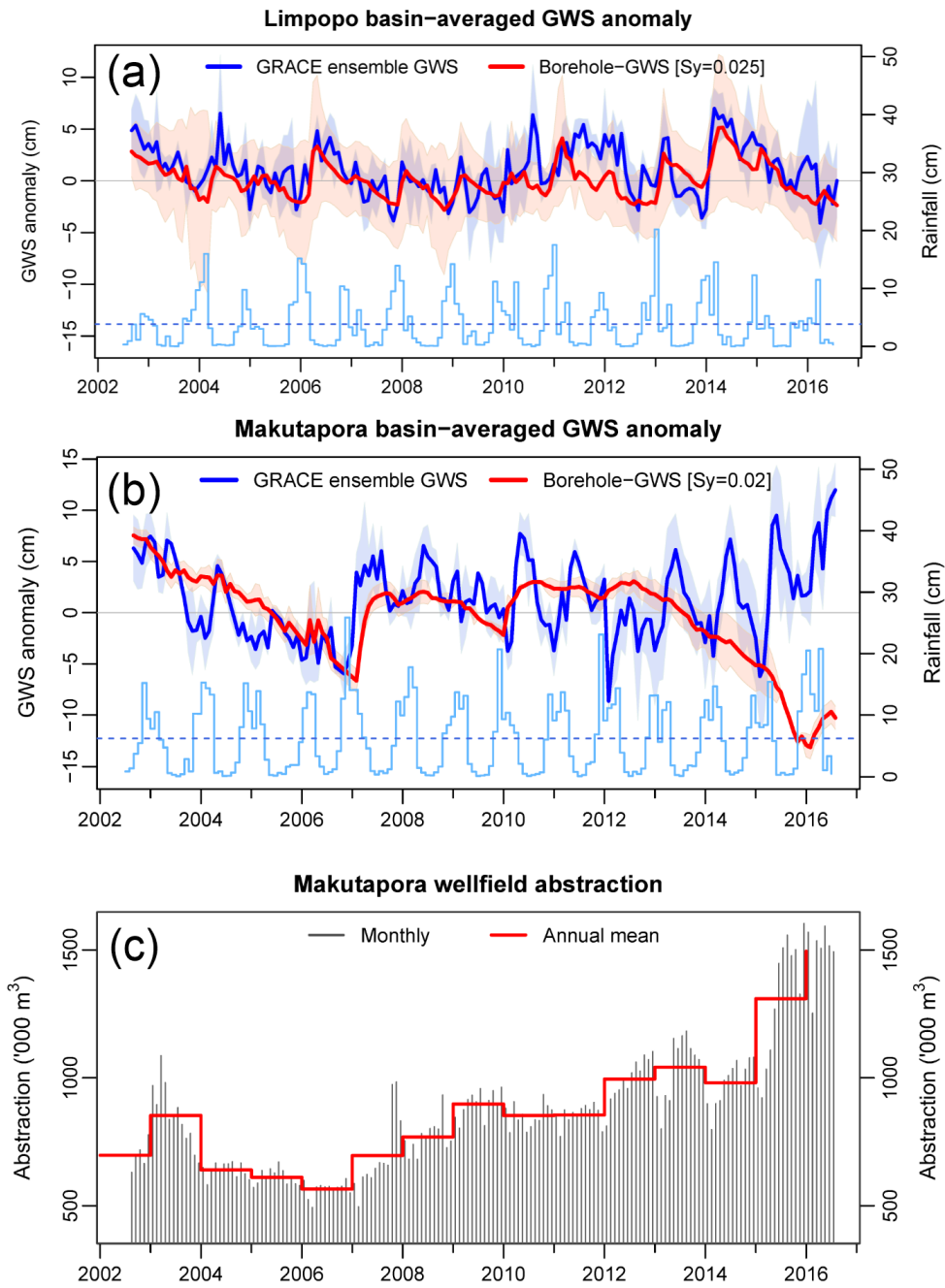


Fig. 4. Water storage anomaly components (cm) over the study domain for the wet season (October-April) of 2015-16 minus long term annual mean 2003-15. (a) GRACE ensemble mean total water storage anomaly ( $\Delta$ TWS, from CSR, JPL-Mascons, GRGS GRACE products); (b) GLDAS ensemble mean soil moisture storage anomaly ( $\Delta$ SMS, 4 land surface models: CLM, NOAH, VIC, MOSAIC); (c) GLDAS ensemble mean surface runoff or surface water storage anomaly ( $\Delta$ SWS, from 4 land surface models: CLM, NOAH, VIC, MOSAIC); and (d) GRACE-GLDAS derived ensemble mean groundwater storage anomaly ( $\Delta$ GWS, from 3 estimates of  $\Delta$ GWS from 3 GRACE products).

867  
868  
869  
870  
871  
872  
873  
874  
875  
876  
877  
878  
879  
880  
881  
882  
883  
884  
885  
886  
887  
888  
889  
890  
891



892 Fig. 5. (a) Time series of estimates of monthly  $\Delta$ GWS anomaly (cm) at Limpopo from August  
893 2002 to July 2016 derived from GRACE averaged over an area approximately  $\sim 120\,000\text{ km}^2$   
894 (bold blue line is the mean of CSR, JPL-Mascons and GRGS products, light blue shading  
895 representing uncertainty across the three products and four LSMs) and piezometry (red line,  
896 mean of all stations, red shading represents uncertainty). Monthly rainfall (from GPCP product,  
897 cm) shown as bars with mean monthly rainfall indicated by a dashed line. (b) As (a) but for  
898 Makutapora. (c) Monthly groundwater abstraction at Makutapora.



1 **The El Niño event of 2015-16: Climate anomalies and their impact on groundwater**  
2 **resources in East and Southern Africa**

3

4 Seshagiri Rao Kolusu<sup>1</sup>, Mohammad Shamsudduha<sup>2,3</sup>, Martin C Todd<sup>1</sup>, Richard G Taylor<sup>2</sup>,  
5 David Seddon<sup>2</sup>, Japhet J Kashaigili<sup>4</sup>, Girma Y Ebrahim<sup>5</sup>, Mark O Cuthbert<sup>2,6</sup>, James P R  
6 Sorensen<sup>7</sup>, Karen G Villholth<sup>5</sup>, Alan M MacDonald<sup>8</sup>, and Dave A MacLeod<sup>9</sup>

7

8 1. Department of Geography, University of Sussex, Brighton, BN1 9QS, UK

9 **Correspondence:**[s.kolusu@sussex.ac.uk](mailto:s.kolusu@sussex.ac.uk) and [sesukulusu@gmail.com](mailto:sesukulusu@gmail.com)

10 2. Department of Geography, University College London, Gower Street, London WC1E  
11 6BT UK

12 3. Institute for Risk and Disaster Reduction, University College London, Gower Street,  
13 London WC1E 6BT, UK

14 4. Sokoine University of Agriculture, Morogoro, Tanzania

15 5. International Water Management Institute, Pretoria, South Africa

16 6. School of Earth and Ocean Sciences, Cardiff University, Main Building, Park Place,  
17 Cardiff, CF10 3AT, UK

18 7. British Geological Survey, Maclean Building, Crowmarsh Gifford, Wallingford,  
19 Oxfordshire OX10 8BB UK

20 8. British Geological Survey, The Lyell Centre, Research Avenue South, Edinburgh  
21 EH14 4AP UK

22 9. Atmospheric Oceanic and Planetary Physics, University of Oxford, OX1 3PU,UK

23

24 **Supplementary Information**

25

26 S1. Climatological context: El Niño and other drivers of climate over EASE/SA, the 2015-16  
27 El Niño event and climate anomalies over SA

28

29 The climatological mean austral summer wet season of October-April rainfall (Fig. S1(a))  
30 shows a maximum extending Northwest-Southeast from Democratic Republic of Congo  
31 (DRC)/Angola in the west, across Zambia, Malawi to northern Mozambique in the East. The  
32 leading mode of interannual variability in rainfall and SPEI-7, is a north/south dipole pattern

33 of opposing anomalies across EASE and SA, with a divide at  $\sim 11^{\circ}\text{S}$ , the approximate mean  
34 latitude of rainfall maximum and is strongly related to ENSO. This structure clearly evidenced  
35 by the leading Empirical Orthogonal Function (EOF) of SPEI-7 (Fig. S1(b)) which explains  
36 21.5% of total variance. The time coefficients correlate strongly with tropical SSTs (Fig. S1(d))  
37 highly characteristic of the ENSO SST anomalies in both the Pacific and Indian Oceans,  
38 notably the SW/NE positive/negative correlation dipole across the southwest/equatorial Indian  
39 Ocean (e.g. Lindesay, 1988; Reason *et al.*, 2000, Lazenby *et al.*, 2016). As such, for Africa  
40 South of the equator the leading mode of climate variability is strongly related to ENSO, with  
41 wet (dry) anomalies during El Niño (la Niña) events across EASE (SA). The EOF pattern is  
42 largely insensitive to the length of choice of months in the wet season. This north-south dipole  
43 response across EASE/SA to ENSO has been well documented previously (Ropelewski and  
44 Halpert, 1987; Janowiak, 1988; Goddard and Graham, 1999; Manatsa *et al.*, 2011), although  
45 the physical mechanisms of teleconnection remain elusive (see Blamey *et al.* 2018 for a  
46 summary).

47

48 The climate anomaly pattern during 2015-16 was highly characteristic of this mode (compare  
49 Figs. 1(a) and S1b). Very strong SST anomalies over the Pacific and elsewhere in the tropics  
50 during 2015-16 (Fig. S1(d)) were associated with a strong north/south dipole in rainfall with  
51 drought in SA (Fig. 1(a)). The socio-economic impacts were pronounced, with much of SA  
52 affected by drought, leading to a regional drought disaster declaration by the Southern Africa  
53 Development Community (SADC). By September 2016, six SADC countries had declared  
54 ‘national drought emergencies’ (Botswana, Namibia Lesotho, Malawi, Swaziland and  
55 Zimbabwe) with drought emergency declared for seven of the South Africa’s nine provinces,  
56 and a temporary red alert also declared for central and Southern provinces of Mozambique  
57 (SADC 2016a). The drought resulted in an extensive loss of crops and livestock, an increase in  
58 food prices, driving an estimated 39 million people into deeper food insecurity (SADC 2016a;  
59 2016b; Archer *et al.*, 2017). Surface water shortages further affected electricity generation and  
60 domestic supply, affecting economic activity and human health (SADC, 2016a; Siderius *et al.*  
61 2018).

62

63 The 2015-16 El Niño was without doubt one of the strongest on record, and by some  
64 indicators was actually the strongest. There are many measures of ENSO strength (see



65 e.g. <https://www.esrl.noaa.gov/psd/enso/dashboard.html>), which provide a mixed picture on  
66 the relative strength of the major events. 2015-16 appears strongest based on the Niño 3.4,  
67 Niño 4 and Bivariate El Niño – Southern Oscillation index, whilst 1997-98 is the strongest  
68 based on the (East pacific Niño 3 and 1+2 SST indices, east Pacific heat content and the  
69 Multivariate El Niño index. However, 2015-16 was certainly more persistent than 1997-98  
70 with many indices turning positive at some time in 2014 related to the El Niño event that was  
71 predicted in 2014 but did not develop fully until 2015-16 (Levine and McPhaden, 2016).

72

73 However, there is substantial diversity in the character of El Niño events, in terms of both (i)  
74 the structure and magnitude of anomalies in the Pacific sector. For example, 2015-16 and 1997-  
75 98 differed in that the former was stronger in the Central Pacific sector (Niño3.4 and Niño SST  
76 region) and the latter in the East Pacific (Niño 1+2 and Niño 3 SST regions) (ii) the state and  
77 evolution of other regional drivers of climate variability which interact with ENSO  
78 teleconnection processes, such that the remote impacts over Africa can be quite variable (e.g.  
79 Ratnam *et al.*, 2014; Preethi *et al.*, 2015, Hoell *et al.*, 2017; Blamey *et al.*, 2018). Across  
80 Southern Africa (SA) multiple regional structures of ocean and atmospheric variability  
81 modulate the impacts of ENSO including the South Indian Ocean dipole (Reason, 2001) as  
82 well as the Angola low and Botswana High atmospheric features (Blamey *et al.*, 2018).  
83 Furthermore, intraseasonal variability associated with the Madden Julian Oscillation, with 30-  
84 60 day timescales can also modulate interannual drivers of variability, particularly over East  
85 Africa (Berhane and Zaitchik, 2014).

86

87 Over East Africa rainfall is more strongly related to the state of the Indian Ocean than to ENSO.  
88 The Indian Ocean Zonal mode (IOZM), an east-west pattern of atmosphere-ocean variability  
89 across the Equatorial Indian ocean, strongly modulates the regional Walker circulation and  
90 hence rainfall over East Africa. During positive IOZM events warmer ocean temperatures in  
91 the equatorial west Indian Ocean and cooler temperatures in the east lead to enhanced rainfall  
92 over EASE, with negative IOZM leading to a reduction in rainfall (see Nicholson 2017 for a  
93 review and references therein). The impact of ENSO on EASE is therefore intimately  
94 connected to the state of the IOZM (Black *et al.*, 2003, Manatsa *et al.*, 2011). During 2015-16  
95 the IOZM was only weakly positive (see SST anomalies in Fig. S1(d)) and the seasonal de-  
96 trended IOZM index (Saji *et al.*, 1999) in 2015-16 was ranked 16<sup>th</sup> out of 150 years. As a result,

97 the mean equatorial zonal Indian Ocean Walker cell with ascent (descent) in the east at  $\sim 100^{\circ}\text{E}$   
98 (west at  $\sim 50^{\circ}\text{E}$ ) of the basin is only weakly perturbed. The zonal cross section over the East  
99 Africa-Indian Ocean sector indicates that enhanced large-scale uplift is limited to a quite  
100 restricted region of EASE from  $\sim 33^{\circ}$ - $40^{\circ}\text{E}$ . In this way, the weak reorganisation of the Indian  
101 ocean Walker circulation led to rather moderate rainfall anomalies over EASE (Section 3.1).

102

## 103 S2. SPEI-7 Intensity-Area-Frequency (IAF) curves and associated return period estimates, and 104 attribution of anthropogenic influence on the SA drought 2015-16

105

106 Droughts are spatially extensive but variable features. We represent the spatial extent using  
107 IAF curves which show the intensity of SPEI-7 water balance anomalies across all spatial scales  
108 within a study domain. IAF curves are independent of the precise spatial patterns of SPEI-7  
109 anomalies, and as such allow us to compare droughts between individual years, and to calculate  
110 the return periods for drought events across scales. This direct comparability of SPEI-7 IAF  
111 curves is valuable since no two drought events have exactly the same spatial pattern. The IAF  
112 curves are derived using the method of Mishra and Cherkauer (2010) separately over the two  
113 study domains of EASE and SA, by calculating the mean SPEI-7 value of grid cells lying within  
114 various areal extent intervals: The areas covered by the lowest (for SA) or highest (for EASE)  
115 5th, 10th, 20th...100th areal percentiles of SPEI grid cell values within the domain area i.e.  
116 when all grid cells are ranked. This allows, for each season, the mean SPEI-7 IAF curve to be  
117 plotted (see Fig. 3).

118

119 We then estimate the return period of the 2015-16 El Niño event by comparing the observed  
120 SPEI-7 IAF curve of 2015-16 with IAF curves representing various ‘benchmark’ return  
121 periods (Fig. 3) and finding the closest match, by least squared error. Estimating these  
122 benchmark return periods of drought events is challenging given the relatively short  
123 observational record for what are relatively long duration events, and indeed because of non-  
124 stationarity in climate records under a changing climate. We address both these challenges in  
125 our approach. To counter the problem of insufficient sampling of the extreme tail of the  
126 distribution, we increase our sample of climate events beyond the observed record using large  
127 ensembles of climate model simulations from the HAPPI experiment (Mitchell *et al.*, 2017).  
128 HAPPI is designed specifically to quantify climate extremes, through the use of relatively

129 high model resolution and large initial-condition ensembles. We use precipitation data from  
130 four atmospheric models, namely HadGEM3, CAM5, MIROC5 and NorESM, (degraded to  
131 common resolution of  $1^\circ$ ) each with 10 ensemble members, run over the period ~1950s-  
132 2010s, forced with observed SSTs and ‘historical’ greenhouse gases and aerosol radiative  
133 forcings. These simulations provide about 2400 years of simulated data, with greater  
134 statistical definition of the extreme tail of the distribution required for the extreme events,  
135 notably the 2015-16 drought over SA which is the strongest on record. As with the  
136 observations we derive the mean SPEI-7 for each areal extent interval (5th, 10th, etc. spatial  
137 percentiles over the domain), for each of the ~2400 model years. Estimation of return periods  
138 is based on the Extreme Value Theory (EVT), widely used for the description of rare climate  
139 events in the extreme tail of the parameter distribution. The Generalized Extreme Value  
140 distribution (GEV) is fitted to the distribution of only the extreme SPEI-7 values, for each  
141 areal extent separately (using maximum likelihood estimation and a chi-squared goodness-of-  
142 fit test, Coles *et al.*, 2001). This distribution of extremes (‘block maxima’) is composed of the  
143 most intense SPEI-7 values (for drought over the SA domain SPEI-7 is multiplied by -1)  
144 within non-overlapping ‘blocks’ of 30 years, a standard climatological period. Then, return  
145 periods are estimated by inverting the resulting GEV cumulative probability distribution for a  
146 range of periods from 30-300 years, for each areal extent separately, providing IAF curves for  
147 benchmark return periods (see Fig. 3). Whilst our approach is similar to previous drought  
148 analyses (e.g. Robeson, 2015) we recognise a number of caveats. First, the estimated return  
149 periods are sensitive to the arbitrary choice of block size and we estimate the uncertainty  
150 associated with this using periods of 25-60 years. Second, whilst the large ensembles  
151 provided by the HAPPI experiment are designed specifically for analysis of extremes they  
152 necessarily provide only a partial representation of the climate variability ‘space’.

153

154 For estimation of return periods shorter than the duration of one ‘block’ (30 years), we  
155 follow Mishra and Cherkauer (2010) and Philip *et al.* (2018) in fitting a distribution to the  
156 historical record of SPEI-7 data. For each areal extent interval (5<sup>th</sup>, 10<sup>th</sup>, etc. spatial  
157 percentiles) we fit a GEV distribution to the 116 historical SPEI-7 data points. We then invert  
158 the cumulative distribution to derive return periods for every spatial percentile, giving a set of  
159 IAF benchmark return period curves. Finally, we conduct all the above IAF curve return  
160 period analysis using SPEI-7 derived with each of the three PET equations and provide the

161 average return period estimates and the associated range to represent this component of  
162 uncertainty.

163

164 It is likely that anthropogenic climate change is, and will continue to, affect large-scale  
165 hydrology. As such, climate risks are changing and non-stationarity in climate records  
166 complicates the interpretation of return periods. However, the IPCC recent assessment report  
167 concludes that there is only low confidence in detection and attribution of observed changes in  
168 drought extremes globally (Bindoff *et al.*, 2013), largely due to uncertainties in distinguishing  
169 relatively small trends in precipitation from decadal variability, especially given limitations in  
170 precipitation data. Nevertheless, attribution of recent temperature rises is robust even down to  
171 the regional/continental scale (Bindoff *et al.*, 2013). In recent probabilistic event attribution  
172 analyses of tropical drought events the contribution of anthropogenic temperature effects is  
173 discernible, in contrast to that of precipitation (Marthews *et al.*, 2015). As such, the full causal  
174 chain from climate anomaly through water balance to agricultural drought is complex and  
175 typically not well represented in models such that attribution of drought remains extremely  
176 challenging. Therefore, here we estimate the effects purely of anthropogenic temperature trends  
177 on drought risk over SA through a simplified attribution experiment. The SPEI-7 IAF return  
178 period analysis above is repeated, but in deriving the benchmark return period curves the  
179 temperature data, used in calculating PET, has the signal of anthropogenic climate change  
180 removed. Specifically, PET is estimated using the HAPPI multi-ensemble mean temperature  
181 from a counterfactual world without human influence on radiative forcing: the ‘natural’ runs,  
182 in which only the natural forcings (solar variability and volcanic aerosols) are provided to the  
183 models. To ensure space-time consistency in all the climate variables whilst changing the  
184 temperature data, we used the 30-year smoothed temperature from the ‘natural’ model runs to  
185 which is added the anomalies of temperature from the ‘historical’ run with respect to a 30-year  
186 running mean. Not that we derive the SPEI-7 over both datasets merged together so that the  
187 effect of the temperature perturbation between the ‘natural’ and ‘historical’ runs is reflected in  
188 the resulting SPEI-7 values, given that the index is standardised across the timeseries. The  
189 benchmark return period IAF curves are then derived from the SPEI-7 values for each dataset  
190 separately. Thus, comparing the estimated SPEI-7 IAF return periods from the climate with  
191 ‘historical’ temperature with those from a counterfactual climate with the ‘natural’ only  
192 temperature, provides an indication of the influence of the anthropogenic temperature trend

193 effects on drought risk over SA. We note that the SPEI is quite temperature dependent through  
194 PET calculation such that other drought indices may yield different sensitivity to warming.

195

196 We must emphasise that this analysis deliberately considers only the effects of the slowly  
197 evolving anthropogenic influence on temperature. We do not consider anthropogenic  
198 influences on rainfall and the other determinants of PET i.e. wind speed, humidity, radiation  
199 budget, no any changes to variability in temperature or any other variables. Further, the  
200 difference in model estimated temperatures between the ‘natural’ and ‘historical’ run will  
201 include the effects not just of anthropogenic radiative forcing but also the surface energy budget  
202 which itself is affected by precipitation and other near surface variables whose response to  
203 radiative forcing we do not consider. However, in utilising a large model ensemble to define  
204 the statistics of extreme events, we retain some features of the probabilistic event attribution  
205 method (e.g. Allen *et al.*, 2003, Stott *et al.*, 2014) but focus solely on that aspect of climate  
206 change (near surface temperatures) for which we have greatest confidence in the ability of  
207 models to represent with credibility.

208

### 209 S3. Groundwater storage estimates from GRACE and LSMs

210

211 To address uncertainty associated with different GRACE processing strategies to resolve  
212  $\Delta$ TWS (Eq. 1) we apply an ensemble mean of three GRACE TWS. Namely, the CSR land  
213 (version RL05.DSTvSCS1409, Swenson and Wahr, 2006; Landerer and Swenson ,2012) and  
214 JPL Global Mascon (version RL05M\_1.MSCNv01, Watkins *et al.*, 2015; Wiese *et al.*, 2015)  
215 solutions, from NASA’s *GRCTellus* data dissemination site (<http://grace.jpl.nasa.gov/data>),  
216 and a third GRGS GRACE solution (CNES/GRGS release RL03-v1) (Biancale *et al.*, 2006)  
217 from the French Government space agency, Centre National D’études Spatiales (CNES).

218

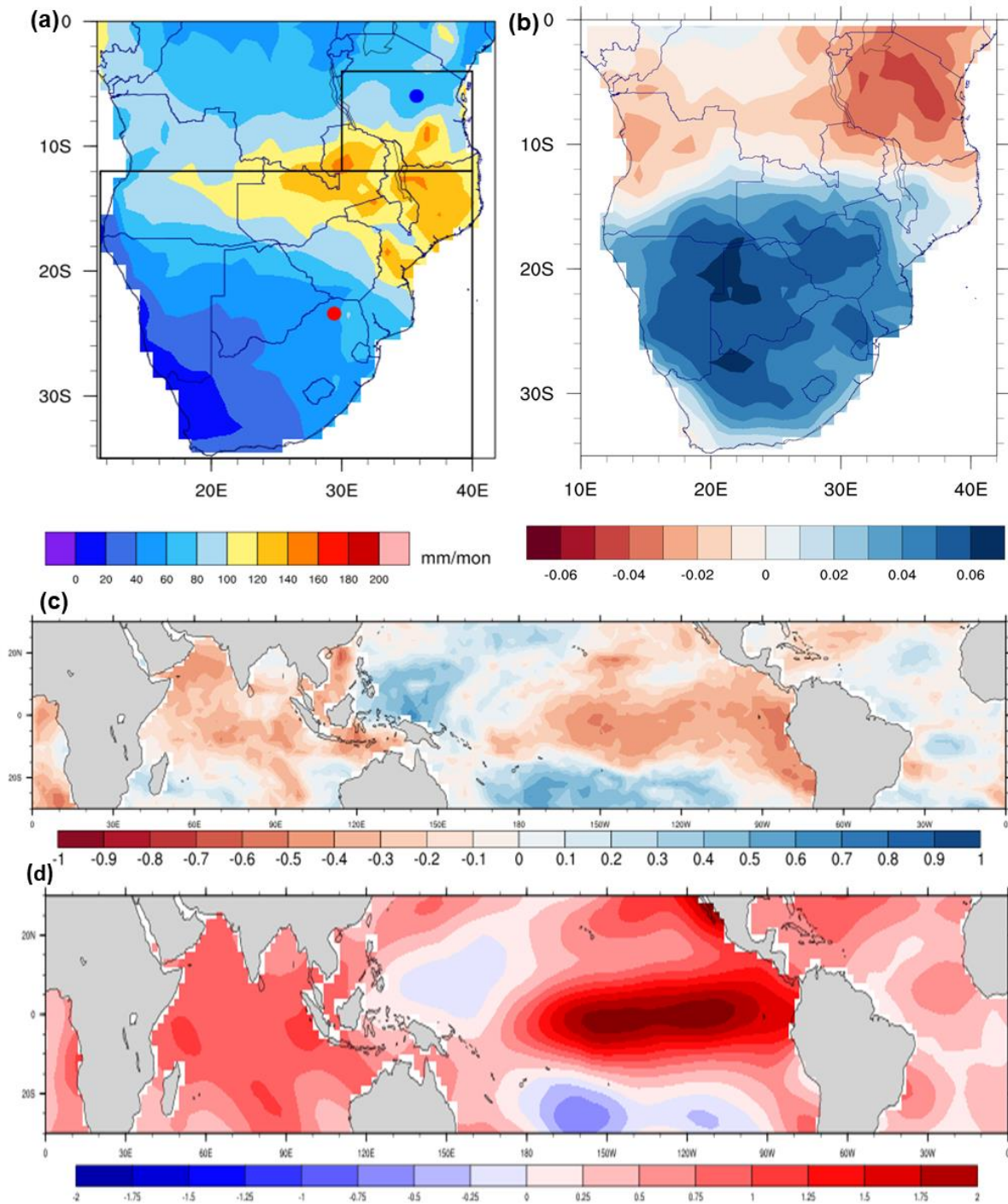
219 *GRCTellus* CSR land solution (version RL05.DSTvSCS1409) is post-processed from spherical  
220 harmonics released by the Centre for Space Research (CSR) at the University of Texas at  
221 Austin. *GRCTellus* gridded datasets are available at a monthly time step and a spatial resolution  
222 of  $1^\circ \times 1^\circ$  (~111 km at equator) though the actual spatial resolution of GRACE footprint is  
223 ~450 km or ~200,000 km<sup>2</sup> (Scanlon *et al.*, 2012). To amplify TWS signals we apply the  
224 dimensionless scaling factors provided as  $1^\circ \times 1^\circ$  bins that are derived from minimising

225 differences between TWS estimated from GRACE and the hydrological fields from the  
226 Community Land Model (CLM4.0) (Landerer and Swenson, 2012). JPL-Mascons (version  
227 RL05M\_1.MSCNv01) data processing involves the same glacial isostatic adjustment  
228 correction but applies no spatial filtering as JPL-RL05M directly relates inter-satellite range-  
229 rate data to mass concentration blocks (mascons) to estimate monthly gravity fields in terms of  
230 equal area  $3^\circ \times 3^\circ$  mass concentration functions in order to minimise measurement errors.  
231 Gridded mascon fields are provided at a spatial sampling of  $0.5^\circ$  in both latitude and longitude  
232 ( $\sim 56$  km at the equator). Similar to *GRCTellus* CSR product, dimensionless scaling factors are  
233 provided as  $0.5^\circ \times 0.5^\circ$  bins (Shamsudduha *et al.*, 2017) that also derive from the Community  
234 Land Model (CLM4.0) (Wiese *et al.*, 2016). The scaling factors are multiplicative coefficients  
235 that minimize the difference between the smoothed and unfiltered monthly  $\Delta$ TWS variations  
236 from the CLM4.0 hydrology model (Wiese *et al.*, 2016). GRGS monthly GRACE products  
237 (version RL03-v1) are processed and made publicly available (<http://grgs.obs-mip.fr/grace>) by  
238 CNES (Shamsudduha *et al.*, 2017). Further details on the Earth's mean gravity-field models  
239 can be found on the CNES official website of GRGS/LAGEOS (<http://grgs.obs-mip.fr/grace/>).  
240 GRACE  $\Delta$ TWS time-series data have some missing records as the satellites are switched off  
241 for conserving battery life (Shamsudduha *et al.*, 2017); these missing records are linearly  
242 interpolated (Shamsudduha *et al.*, 2012).

243

244 To derive  $\Delta$ GWS from GRACE  $\Delta$ TWS (eq. 1) we use simulated soil moisture to represent  
245  $\Delta$ SMS and surface runoff, as a proxy for  $\Delta$ SWS (Mishra *et al.*, 2016), from LSMs within  
246 NASA's Global Land Data Assimilation System (GLDAS). We apply monthly  $\Delta$ SMS and  
247 surface runoff data at a spatial resolution of  $1^\circ \times 1^\circ$  from 4 GLDAS LSMs: The Community  
248 Land Model (CLM, version 2) (Dai *et al.*, 2003), NOAH (version 2.7.1) (Ek *et al.*, 2003), the  
249 Variable Infiltration Capacity (VIC) model (version 1.0) (Liang *et al.*, 2003), and MOSAIC  
250 Mosaic (version 1.0) (Koster and Suarez, 1992). The respective total depths of modelled soil  
251 profiles are 3.4 m, 2.0 m, and 1.9 m and 3.5 m in CLM (10 vertical layers), NOAH (4 vertical  
252 layers), and VIC (3 vertical layers), and Mosaic (3 vertical layers) (Rodell *et al.*, 2004). In the  
253 absence of in situ  $\Delta$ SMS and  $\Delta$ SWS data in the study areas, we apply an ensemble mean of the  
254 4 LSMs-derived  $\Delta$ SMS and  $\Delta$ SWS data in order to disaggregate GRACE  $\Delta$ TWS signals across  
255 our study regions, for the period August 2002 to July 2016, similar to the approach applied for  
256 other locations by Shamsudduha *et al.* (2012, 2017). To help interpretation of these mean

257  $\Delta$ GWS signals we also present the total uncertainty in estimates of  $\Delta$ GWS which result from  
258 the uncertainty in estimates of  $\Delta$ TWS,  $\Delta$ SMS and  $\Delta$ SWS (blue shading in Fig. 5(c)). The  
259 uncertainty in these individual water balance components is shown in Fig. S2 i.e. the range in  
260 estimated GRACE  $\Delta$ TWS across the three retrieval estimates, and the ranges in estimates  
261  $\Delta$ SMS and  $\Delta$ SWS across the four LSMs. Overall, the total uncertainty in  $\Delta$ GWS can be  
262 substantial and receives roughly equal contribution from uncertainty in  $\Delta$ TWS and  $\Delta$ SMS with  
263 uncertainty in  $\Delta$ SWS important only occasionally. There is some indication that during the  
264 periods of greatest  $\Delta$ GWS uncertainty, the  $\Delta$ TWS uncertainty is most important e.g. 2009-10  
265 and 2015-16 at Limpopo. To understand this uncertainty in GRACE  $\Delta$ TWS further we show  
266 the time series of the three individual  $\Delta$ TWS retrievals of CSR, JPL-Mascons and GRGS (Fig.  
267 S3), which we examine in more detail in Section 3.2.2. For further understanding of the  
268 uncertainty in the estimates water storage from LSMs with respect to GRACE readers are  
269 referred to Scanlon *et al.* (2018).



270

271 Fig. S1. (a) Climatological precipitation for the October-April season for the period of 1901-  
 272 2016 ( $\text{mm month}^{-1}$ ). Boxes in Fig. S1(a) show the EASE (small box) and SA (big box) domains  
 273 used in the IAF analysis (see Section 2.1). The blue and red filled circles denote the piezometer  
 274 observation locations at Makutapora, Tanzania and Limpopo, South Africa, respectively. (b)  
 275 Leading mode of interannual October-April variability calculated using the empirical  
 276 orthogonal function (EOF) analysis of de-trended rainfall of GPCP. (c) Correlation between



277 coefficients of EOF1 (Fig. S1(b)) and global SST (October-April mean) 1901-2016. (d) SST  
278 anomalies (K) October-April 2015-16, with respect to 1980-2010 reference period  
279

280

281

282

283

284

285

286

287

288

289

290

291

292

293

294

295

296

297

298

299

300

301

302

303

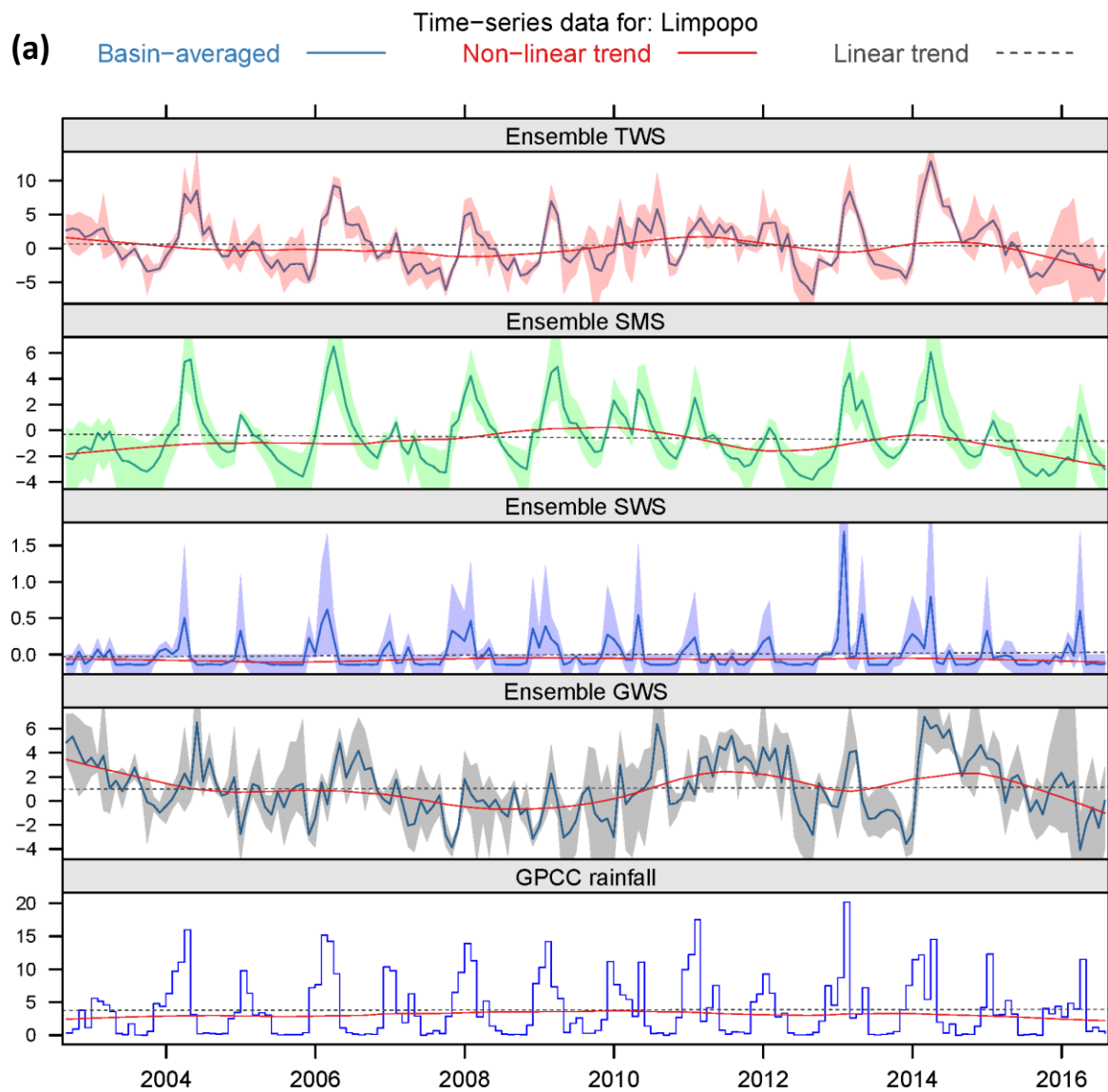
304

305

306

307

308



309  
310  
311  
312  
313  
314  
315  
316  
317  
318  
319  
320  
321  
322  
323  
324  
325  
326  
327  
328  
329  
330  
331  
332  
333  
334  
335  
336  
337  
338  
339  
340  
341  
342  
343  
344  
345

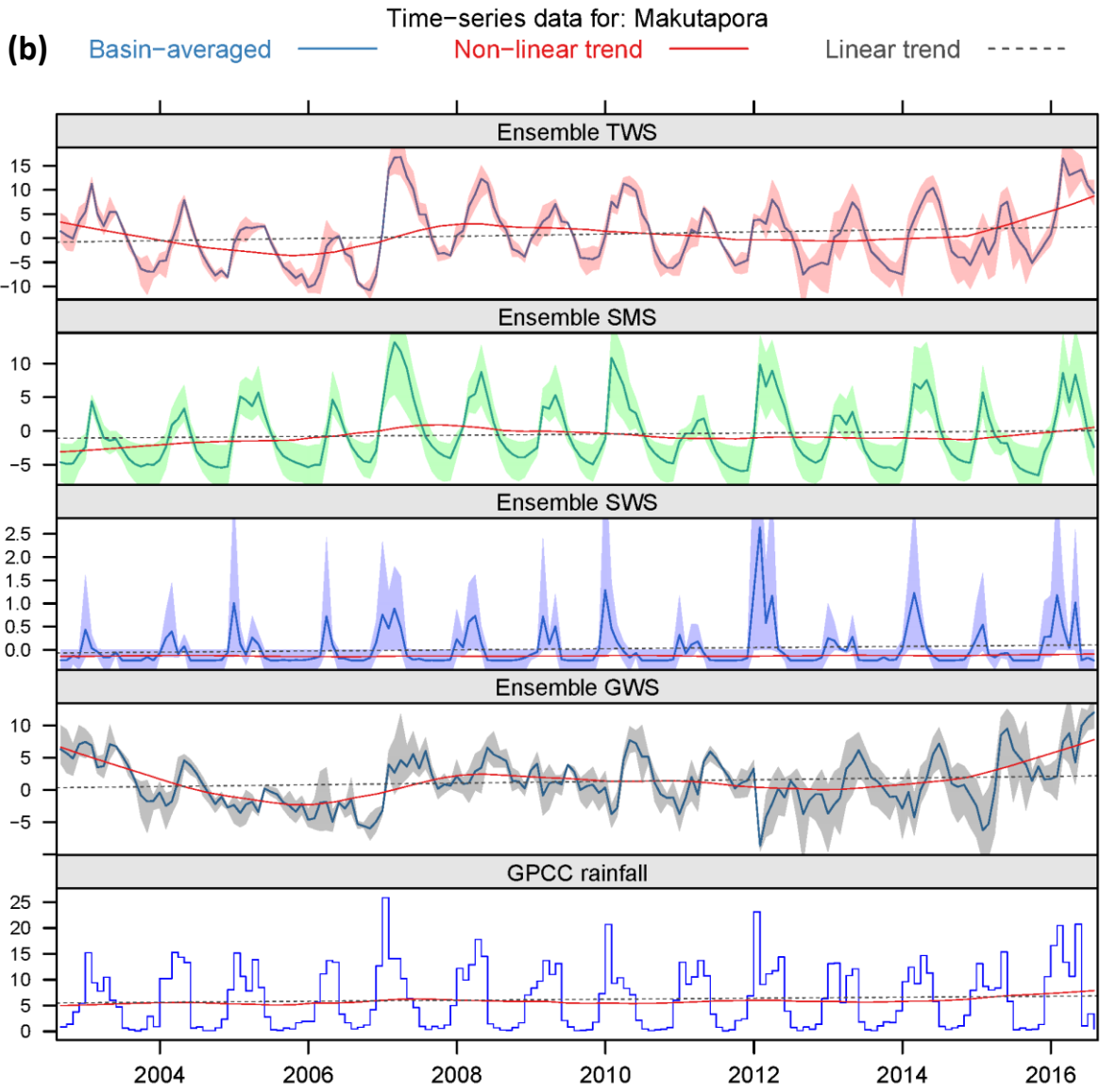
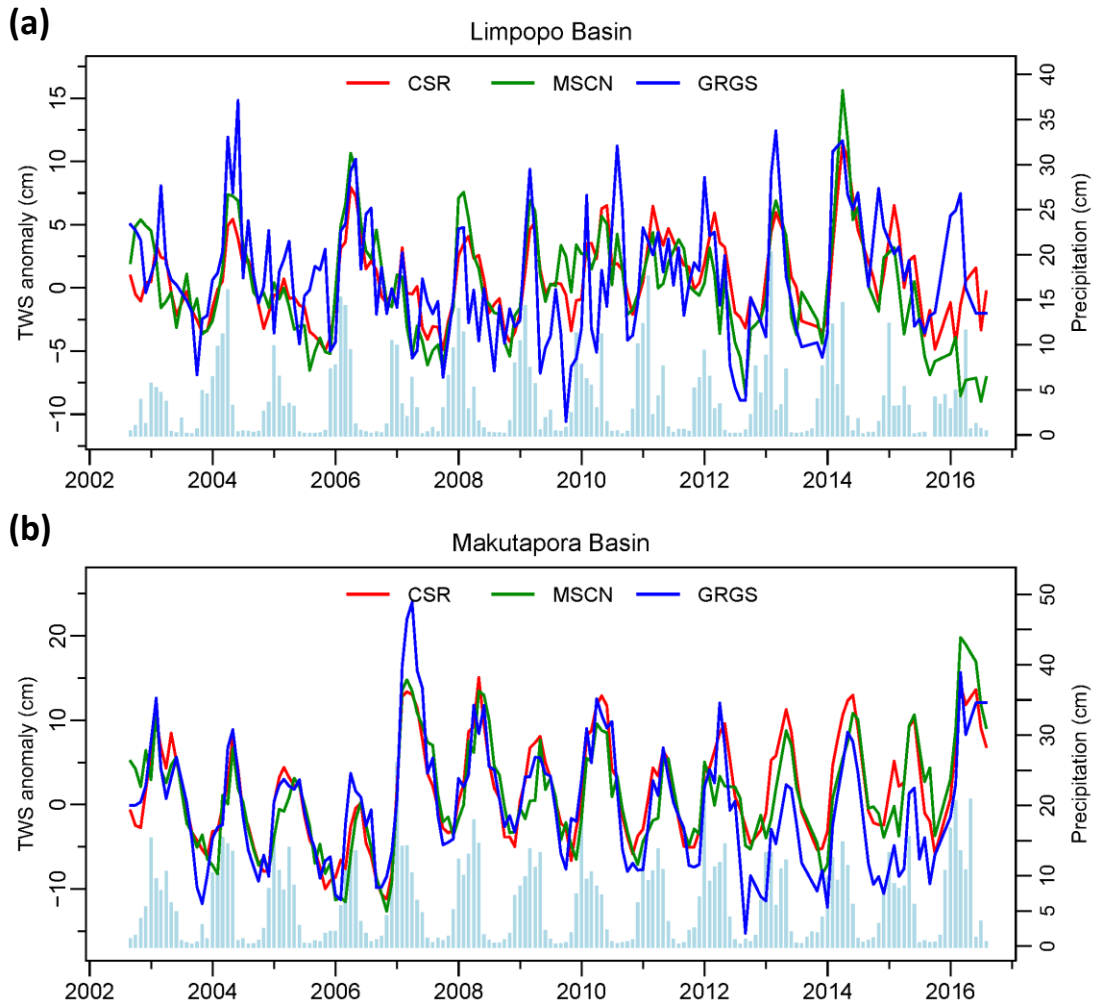


Fig. S2: Time series of monthly estimates of anomalies in the individual components of water balance (lines) and the associated uncertainty range (shaded). From top to bottom TWS from GRACE; SMS and SWS both from LSMs; the residual GWS; observed GPCC rainfall, (all in cm) at (a) Limpopo, and (b) Makutapora.

346  
347  
348  
349  
350  
351  
352  
353  
354  
355  
356  
357  
358  
359  
360  
361  
362  
363  
364  
365  
366  
367  
368  
369  
370



371 Fig. S3: (a) Time series of estimates of monthly  $\Delta$ TWS anomaly (cm) at Limpopo from August  
372 2002 to July 2016 (averaged over an area approximately  $\sim 120\,000\text{ km}^2$ ) derived from the three  
373 individual GRACE retrievals of CSR (red), JPL-Mascons (green) and GRGS (blue). Monthly  
374 rainfall (from GPCP product, cm) shown as bars. (b) As (a) but for Makutapora.

375 **References**

376

377 Allen, M.: Liability for climate change, *Nature*, 421(6926), 891,2003.

378

379 Archer, E. R. M., Landman, W. A., Tadross, M. A., Malherbe, J., Weepener, H., Maluleke,  
380 P., & Marumbwa, F. M.: Understanding the evolution of the 2014–2016 summer rainfall  
381 seasons in southern Africa: Key lessons, *Clim. Risk Manage.*, 16, 22-28, 2017.

382

383 Bindoff, N.L., P.A. Stott, K.M. AchutaRao, M.R. Allen, N. Gillett, D. Gutzler, K. Hansingo,  
384 G. Hegerl, Y. Hu, S. Jain, I.I. Mokhov, J. Overland, J. Perlwitz, R. Sebbari and X. Zhang,:  
385 Detection and Attribution of Climate Change: from Global to Regional. In: Climate Change  
386 2013: The Physical Science Basis. Contribution of Working Group I to the Fifth Assessment  
387 Report of the Intergovernmental Panel on Climate Change [Stocker, T.F., D. Qin, G.-K.  
388 Plattner, M. Tignor, S.K. Allen, J. Boschung, A. Nauels, Y. Xia, V. Bex and P.M. Midgley  
389 (eds.)]. Cambridge University Press, Cambridge, United Kingdom and New York, NY,  
390 USA,2013.

391

392 Berhane, F., & Zaitchik, B: Modulation of daily precipitation over East Africa by the  
393 Madden–Julian oscillation, *J. Climate*, 27(15), 6016-6034, 2014.

394

395 Biancale, R., Lemoine, J-M., Balmino, G., Loyer, S., Bruisma, S., Perosanz, .F, Marty, J-C.,  
396 and Gégout, P.: 3 Years of Geoid Variations from GRACE and LAGEOS Data at 10-day  
397 Intervals from July 2002 to March 2005, CNES/GRGS, 2006

398

399 Black, E., Slingo, J., & Sperber, K. R. :An observational study of the relationship between  
400 excessively strong short rains in coastal East Africa and Indian Ocean SST, *Mon. Weather*  
401 *Rev.*, 131(1), 74-94, 2003.

402

403 Blamey, R. C., Kolusu, S. R., Mahlalela, P., Todd, M. C., & Reason, C. J. C: The role of  
404 regional circulation features in regulating El Niño climate impacts over southern Africa: A  
405 comparison of the 2015/2016 drought with previous events, *Int. J. Climatol.*,,  
406 <https://doi.org/10.1002/joc.5668>, 2018.

407  
408 Coles, S., Bawa, J., Trenner, L., & Dorazio, P.: *An introduction to statistical modelling of*  
409 *extreme values* (Vol. 208), London: Springer, 2001.  
410  
411 Dai, Y., Zeng, X., Dickinson, R. E., Baker, I., Bonan, G. B., Bosilovich, M. G., ... & Oleson,  
412 K. W. :The common land model, *B. Am. Meteorol.*, 84(8), 1013-1024, 2003.  
413  
414 Ek, M. B., Mitchell, K. E., Lin, Y., Rogers, E., Grunmann, P., Koren, V., ... & Tarpley, J. D.  
415 :Implementation of Noah land surface model advances in the National Centers for  
416 Environmental Prediction operational mesoscale Eta model, *J. Geophys. Res.-*  
417 *Atmos.*, 108(D22), 2003.  
418  
419 Goddard, L., & Graham, N. E. :Importance of the Indian Ocean for simulating rainfall  
420 anomalies over eastern and southern Africa, *J. Geophys. Res.-Atmos.*, 104(D16), 19099-  
421 19116, 1999.  
422  
423 Hoell, A., Funk, C., Zinke, J., & Harrison, L.: Modulation of the southern Africa precipitation  
424 response to the El Niño Southern Oscillation by the subtropical Indian Ocean dipole, *Clim.*  
425 *Dynam.*, 48(7-8), 2529-2540, <https://doi.org/10.1007/s00382-016-3220-6>, 2017.  
426  
427 Janowiak, J. E. :An investigation of interannual rainfall variability in Africa. *J. Climate*, 1(3),  
428 240-255, 1988.  
429  
430 Koster, R. D., & Suarez, M. J. : Modeling the land surface boundary in climate models as a  
431 composite of independent vegetation stands, *J. Geophys. Res.-Atmos.*, 97(D3), 2697-2715,  
432 1992.  
433  
434 Landerer, F. W., & Swenson, S. C. :Accuracy of scaled GRACE terrestrial water storage  
435 estimates, *Water Resour. Res.*, 48(4), 2012.  
436  
437 Lazenby, M. J., Todd, M. C., & Wang, Y. : Climate model simulation of the South Indian  
438 Ocean Convergence Zone: mean state and variability, *Clim. Res.*, 68(1), 59-71, 2016.

439  
440 Liang, X., Xie, Z., & Huang, M. :A new parameterization for surface and groundwater  
441 interactions and its impact on water budgets with the variable infiltration capacity (VIC) land  
442 surface model, *J. Geophys. Res.-Atmos.*, 108(D16), 2003.  
443  
444 Lindesay, J. A. : South African rainfall, the Southern Oscillation and a Southern Hemisphere  
445 semi-annual cycle, *J. Climatol.*, 8(1), 17-30, 1988.  
446  
447 Levine, A. F., & McPhaden, M. J.: How the July 2014 easterly wind burst gave the 2015–  
448 2016 El Niño a head start, *Geophys. Res. Lett.*, 43(12), 6503-6510,  
449 <https://doi.org/10.1002/2016GL069204>, 2016.  
450  
451 Manatsa, D., Matarira, C. H., & Mukwada, G.: Relative impacts of ENSO and Indian Ocean  
452 dipole/zonal mode on east SADC rainfall, *Int. J. Climatol.*, 31(4), 558-577, 2011.  
453  
454 Marthews, T. R., Otto, F. E. L., Mitchell, D., Dadson, S. J., & Jones, R. G.: The 2014 drought  
455 in the Horn of Africa: Attribution of meteorological drivers? [in “Explaining Extremes of  
456 2014 from a Climate Perspective”] *B. Am. Meteorol.*, 96(12), S83-S88, 2015.  
457  
458 Mishra, V., & Cherkauer, K. A.: Retrospective droughts in the crop growing season:  
459 Implications to corn and soybean yield in the Midwestern United States, *Agr. Forest*  
460 *Met.*, 150(7-8), 1030-1045, 2010.  
461  
462 Mitchell, D., AchutaRao, K., Allen, M., Bethke, I., Beyerle, U., Ciavarella, A., ... & Ingram,  
463 W. :Half a degree additional warming, prognosis and projected impacts (HAPPI): background  
464 and experimental design, *Geo. Model Develop.*, 10(2), 571-583, [https://doi.org/10.5194/gmd-](https://doi.org/10.5194/gmd-10-571-2017)  
465 [10-571-2017](https://doi.org/10.5194/gmd-10-571-2017), 2017.  
466  
467 Nicholson, S. E.: Climate and climatic variability of rainfall over eastern Africa, *Rev.*  
468 *Geophy.*, 55(3), 590-635, 2017.

469 Philip, S., Kew, S. F., Jan van Oldenborgh, G., Otto, F., O’Keefe, S., Hausteine, K., ... &  
470 Singh, R. Attribution analysis of the Ethiopian drought of 2015, *J. Climate*, 31(6), 2465-  
471 2486, 2018.

472

473 Preethi, B., Sabin, T. P., Adedoyin, J. A., & Ashok, K.: Impacts of the ENSO Modoki and  
474 other tropical Indo-Pacific climate-drivers on African rainfall, *Sci. Rep.*, 5, 16653, 2015.

475

476 Ratnam, J. V., Behera, S. K., Masumoto, Y., & Yamagata, T. :Remote effects of El Niño and  
477 Modoki events on the austral summer precipitation of southern Africa, *J. Climate*, 27(10),  
478 3802-3815, 2014.

479

480 Reason, C. J. C., Allan, R. J., Lindesay, J. A., & Ansell, T. J. : ENSO and climatic signals  
481 across the Indian Ocean basin in the global context: Part I, Interannual composite  
482 patterns. *International J. Climatol.*, 20(11), 1285-1327, 2000.

483

484 Reason, C. J. C. : Subtropical Indian Ocean SST dipole events and southern African  
485 rainfall, *Geophys. Res. Lett.*, 28(11), 2225-2227, 2001

486

487 Robeson, S. M. :Revisiting the recent California drought as an extreme value, *Geophys. Res.*  
488 *Lett.*, 42(16), 6771-6779, 2015.

489

490 Rodell, M., Houser, P. R., Jambor, U. E. A., Gottschalck, J., Mitchell, K., Meng, C. J., ... &  
491 Entin, J. K. ;The global land data assimilation system, *B. Am. Meteorol.*, 85(3), 381-394,  
492 2004.

493

494 Ropelewski, C. F., & Halpert, M. S. : Global and regional scale precipitation patterns  
495 associated with the El Niño/Southern Oscillation. *Mon. Weather Rev.*, 115(8), 1606-1626,  
496 1987.

497

498 SADC 2016a: SADC regional situation update on El Nino-induced drought, Issue 02, 12th  
499 September 2016, SADC, 12pp, available at:

500 ,[https://www.sadc.int/files/9514/7403/9132/SADC\\_Regional\\_Situation\\_Update\\_No-2\\_16-](https://www.sadc.int/files/9514/7403/9132/SADC_Regional_Situation_Update_No-2_16-)  
501 09-2016.pdf, 2016.

502

503 SADC 2016b: SADC Regional Vulnerability Assessment and Analysis Synthesis Report:  
504 State of Food Insecurity and Vulnerability in the Southern African Development Community,  
505 SADC, 66pp, available at: [https://www.sadc.int/files/9014/7911/5767/SADC\\_RVAA-](https://www.sadc.int/files/9014/7911/5767/SADC_RVAA-)  
506 [August-Final-Web.pdf](https://www.sadc.int/files/9014/7911/5767/SADC_RVAA-), 2016

507

508 Saji, N. H., Goswami, B. N., Vinayachandran, P. N., & Yamagata, T.: A dipole mode in the  
509 tropical Indian Ocean, *Nature*, 401(6751), 360, doi:10.1038/43854, 1999.

510

511 Scanlon, B. R., Longuevergne, L. , and Long, D.: Ground referencing GRACE satellite  
512 estimates of groundwater storage changes in the California Central Valley, USA *Water*  
513 *Resour. Res.*, 48 W04520, 2012.

514

515 Scanlon, B. R., Zhang, Z., Save, H., Sun, A. Y., Schmied, H. M., van Beek, L. P., ... &  
516 Longuevergne, L. : Global models underestimate large decadal declining and rising water  
517 storage trends relative to GRACE satellite data, *P. Nat. Acad. Sci*, 201704665,  
518 <https://doi.org/10.1073/pnas.1704665115>, 2018.

519

520 Shamsudduha, M., Taylor, R. G., & Longuevergne, L.: Monitoring groundwater storage  
521 changes in the highly seasonal humid tropics: Validation of GRACE measurements in the  
522 Bengal Basin, *Water Resour. Res.*, 48(2), 2012.

523

524 Shamsudduha, M., Taylor, R. G., Jones, D., Longuevergne, L., Owor, M., & Tindimugaya, C.  
525 :Recent changes in terrestrial water storage in the Upper Nile Basin: an evaluation of  
526 commonly used gridded GRACE products, *Hydrol. Earth Syst. Sci.*, 21(9), 4533-4549,  
527 <https://doi.org/10.5194/hess-21-4533-2017>, 2017.

528

529 Siderius, C., Gannon, K. E., Ndiyoi, M., Opere, A., Batisani, N., Olago, D., ... & Conway, D.  
530 :Hydrological response and complex impact pathways of the 2015/2016 El Niño in Eastern  
531 and Southern Africa, *Earth's Fut.*, 6(1), doi:10.1002/2017EF000680,2-22, 2018.



532  
533 Stott, P. A., Hegerl, G. C., Herring, S. C., Hoerling, M .P., Peterson, T. C., Zhang, X., and  
534 Zwiers, F. W.: Introduction to explaining extreme events of 2013 from a climate perspective,  
535 *B. Am. Meteorol.*, 95 S1–S3, 2014  
536  
537 Swenson, S., & Wahr, J.: Post-processing removal of correlated errors in GRACE  
538 data, *Geophys. Res. Lett.*, 33(8), 2006.  
539  
540 Taylor, R. G., Todd, M. C., Kongola, L., Maurice, L., Nahozya, E., Sanga, H., & MacDonald,  
541 A. M. : Evidence of the dependence of groundwater resources on extreme rainfall in East  
542 Africa, *Nature Clim. Cha.*, 3(4), 374, 2013.  
543  
544 Vicente-Serrano, S. M., Beguería, S., & López-Moreno, J. I. : A multiscalar drought index  
545 sensitive to global warming: the standardized precipitation evapotranspiration index, *J.*  
546 *Climate*, 23(7), 1696-1718, 2010.  
547  
548 Watkins, M. M., Wiese, D. N., Yuan, D. N., Boening, C., & Landerer, F. W. : Improved  
549 methods for observing Earth's time variable mass distribution with GRACE using spherical  
550 cap mascons, *J. Geo. Res.: Solid Earth*, 120(4), 2648-2671, 2015.  
551  
552 Wiese, D. N., Yuan, D-N., Boening, C., Landerer, F. W., and Watkins, M. M.: JPL GRACE  
553 Mascon Ocean, Ice, and Hydrology Equivalent Water Height JPL RL05M.1. Ver. 1  
554 PO.DAAC CA USA, 2015.  
555  
556 Wiese, D. N., Landerer, F. W., and Watkins, M. M.: Quantifying and reducing leakage errors  
557 in the JPL RL05M GRACE mascon solution, *Water Resour.Res.*, 52, 7490-7502, 2016.